NASA/TM-2006-214496

Anomalous Shocks on the Measured Near-Field Pressure Signatures of Low-Boom Wind-Tunnel Models

Robert J. Mack
Langley Research Center, Hampton, Virginia

August 2006

The NASA STI Program Office . . . in Profile

Since its founding, NASA has been dedicated to the advancement of aeronautics and space science. The NASA Scientific and Technical Information (STI) Program Office plays a key part in helping NASA maintain this important role.

The NASA STI Program Office is operated by Langley Research Center, the lead center for NASA's scientific and technical information. The NASA STI Program Office provides access to the NASA STI Database, the largest collection of aeronautical and space science STI in the world. The Program Office is also NASA's institutional mechanism for disseminating the results of its research and development activities. These results are published by NASA in the NASA STI Report Series, which includes the following report types:

- TECHNICAL PUBLICATION. Reports of completed research or a major significant phase of research that present the results of NASA programs and include extensive data or theoretical analysis. Includes compilations of significant scientific and technical data and information deemed to be of continuing reference value. NASA counterpart of peer-reviewed formal professional papers, but having less stringent limitations on manuscript length and extent of graphic presentations.

- TECHNICAL MEMORANDUM. Scientific and technical findings that are preliminary or of specialized interest, e.g., quick release reports, working papers, and bibliographies that contain minimal annotation. Does not contain extensive analysis.

- CONTRACTOR REPORT. Scientific and technical findings by NASA-sponsored contractors and grantees.

- CONFERENCE PUBLICATION. Collected papers from scientific and technical conferences, symposia, seminars, or other meetings sponsored or co-sponsored by NASA.

- SPECIAL PUBLICATION. Scientific, technical, or historical information from NASA programs, projects, and missions, often concerned with subjects having substantial public interest.

- TECHNICAL TRANSLATION. English-language translations of foreign scientific and technical material pertinent to NASA's mission.

Specialized services that complement the STI Program Office's diverse offerings include creating custom thesauri, building customized databases, organizing and publishing research results ... even providing videos.

For more information about the NASA STI Program Office, see the following:

- Access the NASA STI Program Home Page at ***http://www.sti.nasa.gov***

- E-mail your question via the Internet to help@sti.nasa.gov

- Fax your question to the NASA STI Help Desk at (301) 621-0134

- Phone the NASA STI Help Desk at (301) 621-0390

- Write to:
  NASA STI Help Desk
  NASA Center for AeroSpace Information
  7121 Standard Drive
  Hanover, MD 21076-1320

NASA/TM-2006-214496

Anomalous Shocks on the Measured Near-Field Pressure Signatures of Low-Boom Wind-Tunnel Models

Robert J. Mack
Langley Research Center, Hampton, Virginia

National Aeronautics and
Space Administration

Langley Research Center
Hampton, Virginia 23681-2199

August 2006

Available from:

NASA Center for AeroSpace Information (CASI)
7121 Standard Drive
Hanover, MD 21076-1320
(301) 621-0390

National Technical Information Service (NTIS)
5285 Port Royal Road
Springfield, VA 22161-2171
(703) 605-6000

Summary

Unexpected shocks, found on the measured pressure signatures generated by low-boom wind-tunnel models, prompted questions about the capabilities of the design methods, the pressure signature measurement techniques, and the quality of measurements in the flow field very near lifting wing/body models. Some of these unexpected shocks were the result of component integration methods. Others were attributed to the three-dimension nature of the flow around a lifting, wing/body, wind-tunnel model, to inaccuracies in the prediction of the area-ruled lift, or to wing-tip stall effects. This report discussed the low-boom model data where these unexpected shocks were initially observed, the physics of the lifting wing/body model's flow field, the wind-tunnel data used to evaluate the applicability of methods for calculating equivalent areas due to lift, the performance of lift prediction codes, and tip stall effects so that the cause of these shocks could be determined.

Introduction

During the past forty years of sonic-boom research, methods have been developed for the implementation of sonic-boom theory, the prediction of ground overpressures, and the conceptual design of low-boom aircraft. These prediction codes and design methods were tested by building models, measuring their pressure signatures in the wind tunnel, and comparing measured and predicted pressure signatures. Early sonic-boom studies were done with body-of-revolution models having a wide range of geometric shapes, and with models having a wing-body or a conceptual aircraft geometry, references 1 to 6. They were designed and analyzed with aerodynamic and sonic-boom codes, references 7 to 10, developed in the years from the late 1950's to the early 1970's. The first sonic-boom models were small so the capabilities of the Whitham and Walkden far-field shock generation and propagation theories, references 11 and 12, could be tested and validated in the test sections of available supersonic wind-tunnel facilities. Favorable results of these wind-tunnel tests lead to larger models which changed the nature of the wind-tunnel flow field and measured data from almost far-field to near-field.

Pressure signatures generated by slender bodies of revolution, such as those in references 5 and 6, could be reasonably well predicted with Whitham-Walkden theory when the separation distance was greater than 5 to 10 body lengths. Wing-fuselage models, on the other hand, generated near-field wind-tunnel pressure signatures that could not be accurately predicted with Whitham-Walkden theory along their entire length because the wing lift could be reasonably represented by equivalent area bodies only at, or approaching, far-field distances.

During the measurements of near-field pressure signatures with the larger, low-boom, wing / fuselage, wind-tunnel models, unexpected shocks were measured; anomalous features not predicted by methods used to analyze and tailor the model's low-boom lift and volume geometry. It was these unexpected shocks that prompted questions about whether they were a result of shortcomings the design and analysis methods capabilities, inaccuracies in the performance prediction methods, or due to the physical nature of the three-dimensional near-field flow. These unexpected shocks, the wind-tunnel models that generated them, and the questions they provoked, will be analyzed and discussed in this report.

Nomenclature

A	wing aspect ratio, b^2 / S
$A_{e,c}$	source strength term for the slender cone volume
$A_{e,w}$	dipole strength term for the slender wing at small angle of attack
b	wing span, ft or in
$b(\xi)$	local span at distance ξ from wing apex, ft or in
C_L	lift coefficient
$C_{L,CRUISE}$	cruise lift coefficient
h	cruise altitude or separation distance, ft or in
I	impulse: maximum positive value of $\int(\Delta p)dx$, psf-in, psf-ft
I_c	impulse from the volume of a slender conical body, psf-in, psf-ft
I_w	impulse from the lift on a slender delta wing, psf-in, psf-ft
l	overall, wing lifting, or root chord length, ft or in
L/D	lift to drag ratio
M	Mach number
p	ambient pressure, psf
Δp	incremental free-stream pressure, psf
S	reference or wing area, ft^2 or in^2
u	longitudinal perturbation velocity made nondimensional with the free-stream velocity
u_c	longitudinal perturbation velocity from a slender cone at supersonic speed made nondimensional with the free-stream velocity, equation (2)
u_w	longitudinal perturbation velocity from a slender delta wing at supersonic speed, made nondimensional with the free-stream velocity, equation (3a)
x	longitudinal distance in the direction along the wing chord, ft or in
x'/c	distance behind wing leading edge to chord ratio
Δx	increment between near-field and far-field Mach cone intersections, used interchangeably with $\Delta\xi$, ft or in
y	distance along the semi-span direction, ft or in
z	distance normal to the x - y plane, ft or in
α	angle of attack, deg

β	Mach number parameter, $\sqrt{M^2 - 1}$
γ	ratio of specific heats, 1.4 for air
ζ	variable in the u_c and u_w perturbation velocity relations, equation (4b)
η	distance along the semi-span direction in the wing plane, ft or in
θ	meridian angle measured from symmetry plane above the body, deg
Λ	wing leading edge sweep angle, deg
μ	Mach angle, $\sin^{-1}(1.0 / \mathrm{M})$, deg
ξ	distance along the root chord of the delta wing, ft or in
$\Delta\xi$	increment between near-field and far-field Mach cone intersections, used interchangeably with Δx , ft or in

Anomalous Shocks

During the 1960's and 1970's, several sonic-boom analysis, aerodynamic design, and mission performance computer codes were developed to predict the ground overpressures of vehicles in supersonic-cruise flight as well as the measured pressure signatures of research wind-tunnel models. As these codes came on line, low-boom studies were performed to apply, test, and evaluate these new or updated theories and methods.

One study of wing-fuselage models, reference 13, was performed in the late 1970's. Others, references 14 to 19, were carried out in the late 1980 - 1995 period after the start of the High Speed Research (HSR) project, and another, references 20 and 21, was done after the HSR program ended. During the measurement of pressure signatures from some of the larger wind-tunnel wing/fuselage models (12 to 16 inches in length) at cruise angle of attack, unexpected shocks appeared. Insufficient accuracy in the prediction of the lift distribution was identified as the major factor in the sonic-boom study of reference 13. This deficiency lead to the development of the Modified Linear Theory wing performance prediction code, reference 22, which became the wing performance analysis method of choice when low-boom conceptual aircraft and wind-tunnel models were designed in the follow-on sonic-boom studies.

While some of these unexpected shocks were caused by inaccuracies in the lift distribution prediction method, others were attributed to the location of the wind-tunnel model's engine nacelles, reference 15. Some of the models had wings, fuselages, nacelles, and fins that were scaled versions of the full scale concept. With some nacelle locations, the concept's ground pressure signature would have stronger nose shocks as the result of nacelle shocks coalescing with the original low-boom nose shock as the ensemble of disturbances propagated down through the atmosphere. Once the cause of these shocks was identified, a revised, low-boom nacelle integration method, reference 23, was developed to eliminate, or at least minimize, their detrimental effects on the conceptual aircraft's low-boom flow field.

Other unexpected shocks and their causes were not so easily identified. The measurement of pressure signatures in two subsequent sonic-boom studies, references 19 and 21, re-awakened doubts about the accuracy of the lift-distribution prediction code. A sonic-boom workshop paper, reference 24, suggested near-field effects were important, but these comments were directed at the methodology of existing pressure signature extrapolation methods. Now, the magnitude and extent of these near-field effects were suspected of being more important and widespread than formerly thought.

In response to accuracy doubts, the Modified Linear Theory wing performance prediction method had been developed and used to calculate the lift equivalent area distributions. Still, anomalous shocks appeared in the measured pressure signatures generated by low-boom-tailored lifting wing-body models. Some of these shocks were similar to those on the pressure signatures presented and analyzed in reference 13.

In the following sections, the low-boom concepts and wind-tunnel models reported in references 13 to 21, along with their measured pressure signature data, will be presented, analyzed, and discussed. Anomalous shocks, seen during the wind-tunnel measurement of low-boom model pressure signatures from these models, will be identified. Possible reasons for their appearance on the measured near-field pressure signatures of low-boom models will be presented and discussed.

Pressure Signature Data

Several low-boom models gave pressure signatures with anomalous shocks. Two low-boom concepts (described in Appendix A), reference 13, were designed to assess Seebass and George low-boom minimization, reference 25. Wind-tunnel models with ducted nacelles mounted under the wings were built, and pressure signatures were measured for comparison with theory.

The wind-tunnel models of three follow-on High Speed Civil Transport (HSCT) concepts, references 16 to 18, also had ducted nacelles. Two of the follow-on concepts had the engine nacelles mounted under the wings, references 16 and 17, but, the third concept and model, references 18 and 19, had nacelles mounted on the aft fuselage, well behind the wing trailing edge. Due to the unique nature of the pressure signatures generated by this third model, only this concept, the HSCT-10B, its wind-tunnel model, and wind-tunnel data is discussed in this report.

A subsequent study of low-boom Supersonic Business Jet (SBJ) concepts also involved a concept with aft-fuselage mounted engine nacelles, reference 20. Measured pressure signatures from the wind-tunnel model of this concept, reference 21, as well as from models of the previously mentioned three concepts are presented, analyzed, and discussed in the following sections.

Mach 2 Concept and Model

A three-view sketch of the first of the two theory-validation concepts, the Mach 2 concept, is shown in figure 1.

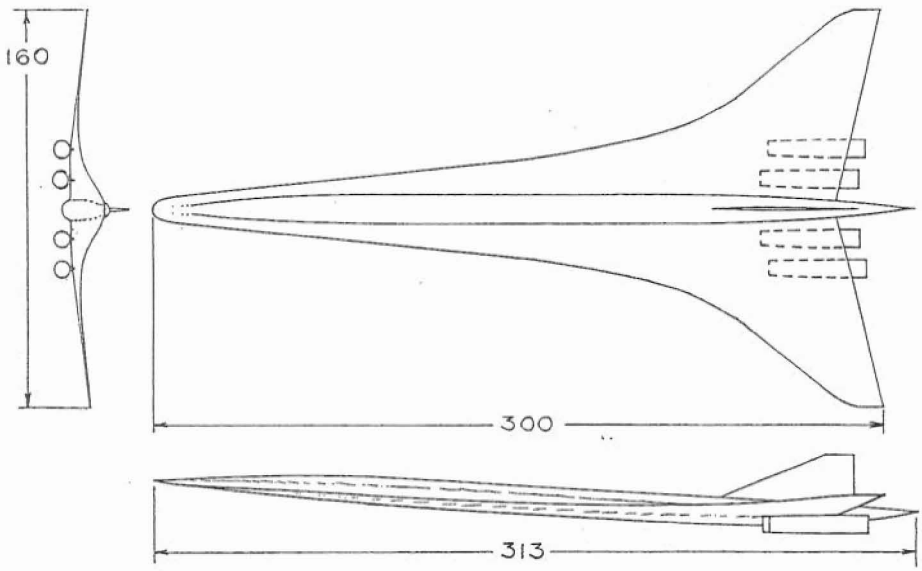

Figure 1. Three view of the Mach 2 theory-validation concept.

The wind-tunnel model of the Mach 2 concept, built to 1:300 scale out of stainless steel, was 12 inches long, and had an integral fuselage/sting/balance. Four body-of-revolution ducted nacelles with sharp inlet lips were made from stainless steel tubing. They were mounted on short struts and attached under the wing near the trailing edge.

Measured pressure signatures, like the one seen in figure 2, were generated by the wind-tunnel model of the Mach 2 concept shown in figure 1.

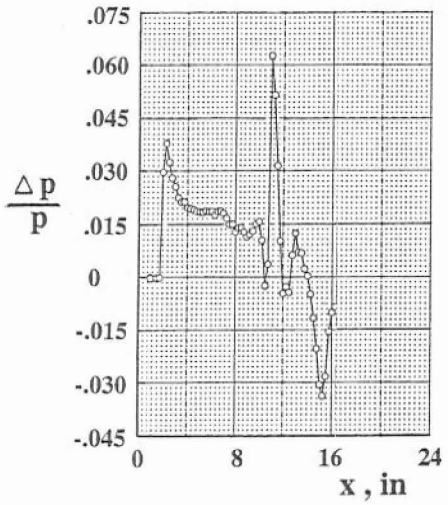

Figure 2. Mach 2 wind-tunnel model pressure signature with nacelles. M = 2.0, h = 12 inches, $C_L = C_{L,CRUISE}$.

Note the difference between the pressure signature in figure 2 and the pressure signature in figure 3, which was measured when the model's nacelles were removed.

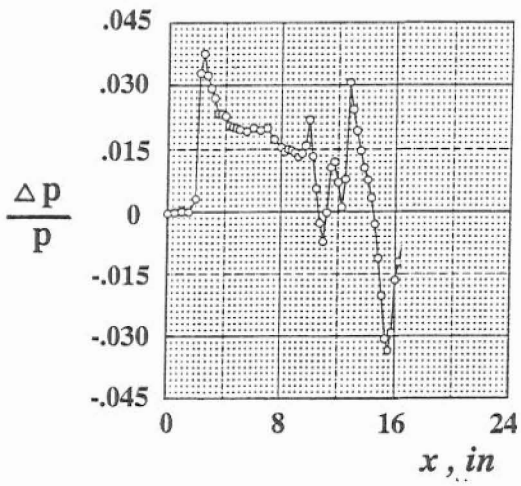

Figure 3. Mach 2 wind-tunnel model pressure signature without nacelles. M = 2.0, h = 12 inches, $C_L = C_{L,CRUISE}$.

Figure 3 shows the strong shock, aft of the nose shock in figure 2, disappeared when the nacelles were removed from the model. However, that extra strong shock was unexpected because the concept's and the wind-tunnel model's lift and volume equivalent areas had been tailored by applying the Seebass and George minimization methods to obtain a "flattop" pressure signature in the wind tunnel test section as well as on the ground. These test results would be repeated when pressure signatures from the Mach 3 concept were measured.

Mach 3 Concept and Model

The second theory validation concept, the Mach 3 concept, was another simple wing-fuselage configuration. Its wing, like the wing on the Mach 2 concept, was constrained and shaped only to meet and validate Seebass and George low-boom minimization constraints. However, before the low-boom tailoring was performed, the initial wing span and length were reduced by 10 percent to bring the area closer to the wing area on the Mach 2 concept. A three view sketch of the Mach 3 concept with its resized wing is shown in figure 4.

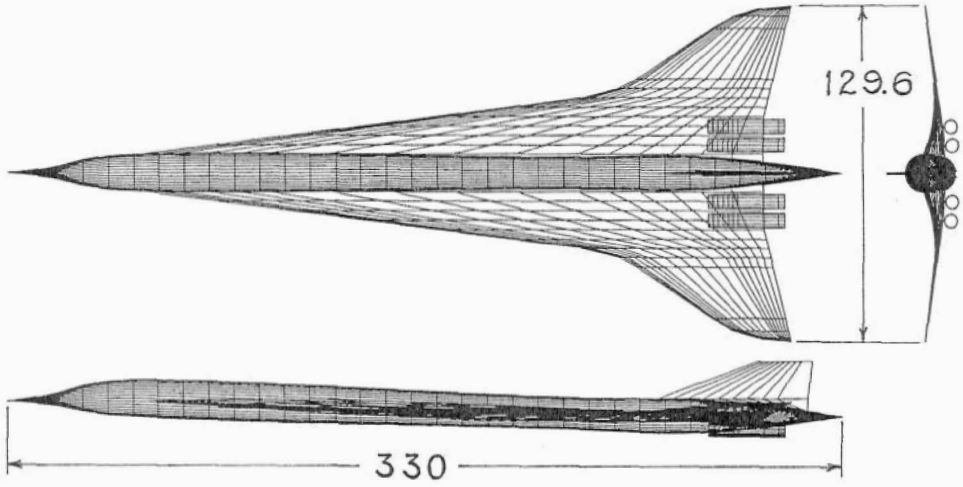

Figure 4. Three view sketch of the resized Mach 3 theory-validation concept.

The wind-tunnel model of the Mach 3 concept, like the wind-tunnel model of the Mach 2 concept, was built of stainless steel to a scale of 1:300. It was 12 inches long, had four body-of-revolution ducted nacelles, and an integral fuselage/sting/balance. In figure 5, a measured pressure signature from the Mach 3 wind-tunnel model is shown with $C_L = C_{L,CRUISE}$.

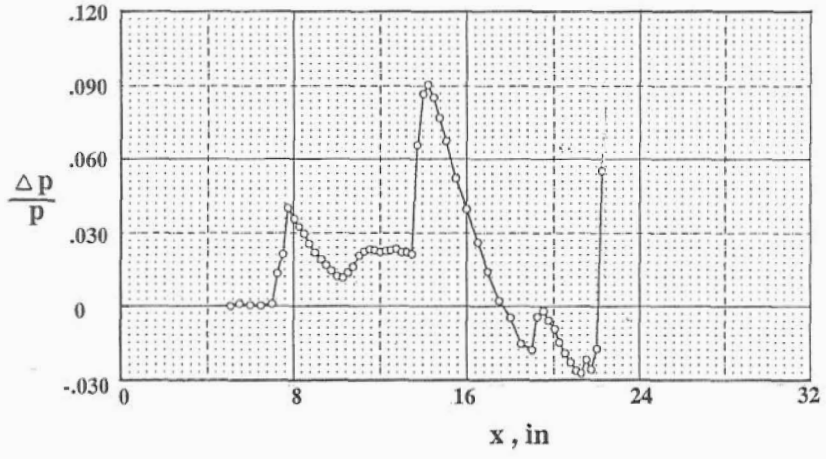

Figure 5. Pressure signature from the Mach 3 model with nacelles. M = 2.96, h = 8.5 inches, $C_L = C_{L,CRUISE}$.

The nacelles-on pressure signature from the Mach 3 model was similar to the nacelles-on pressure signature from the wind-tunnel model of the Mach 2 concept. When the nacelles were removed from the Mach 3 model, the pressure signature shown in figure 6 was measured.

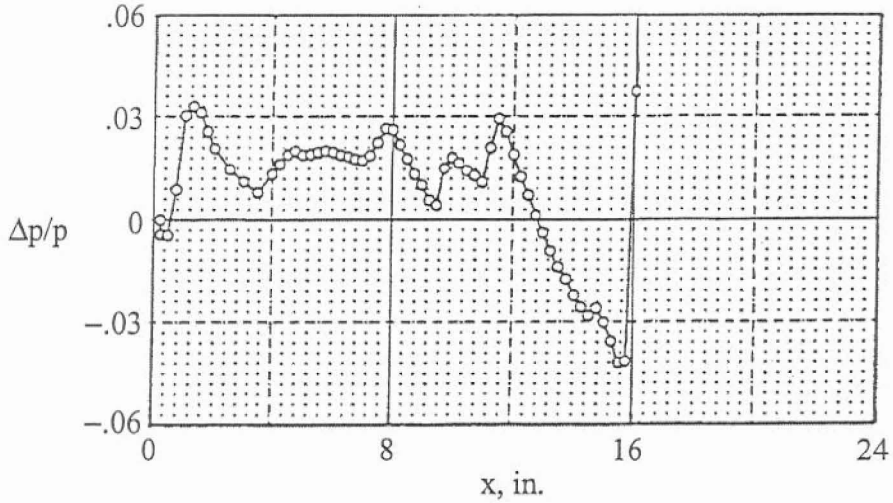

Figure 6. Pressure signature from the Mach 3 model without nacelles. M = 2.96, h = 8.5 inches, $C_L = C_{L,CRUISE}$.

The pressure signature in figure 6, like the one in figure 3, does not have the extra strong shock because the ducted nacelles have been removed. These anomalous shocks appeared in the two models' pressure signatures because the shocks that formed at the nacelle inlet lips and propagated into the flow field were enhanced by their reflection from the lower surface of the wing. Based on these results, it was concluded that the design and analysis methods used at the time underestimated the strengths of these reflected lip shocks.

These measured pressure signatures, generated by models of concepts with under-the-wing engine nacelles, demonstrated the existing design, analysis, and nacelle integration methods needed to be re-evaluated, and if necessary, modified to account for these extra shocks. The re-evaluation and subsequent modifications were applied in the following year, as outlined in reference 23. Then, they were incorporated into the appropriate sonic-boom analysis methods, concept design strategies, and nacelle integration techniques.

HSCT-10B Concept and Model

Three follow-on low-boom concepts, references 16 to18, were designed with computer codes incorporating the updated and revised sonic-boom analysis, concept design, and nacelle integration methods. These concepts were the Boeing B935, the Langley LB16, and the Langley HSCT-10B. Descriptions of these three concepts are found in Appendix B.

Wind-tunnel models of these concepts were built to 1:300 scale, and their pressure signatures were measured in Langley Research Center's Unitary Plan Wind Tunnel Facility. Examples of the pressure signatures from the HSCT-10B concept wind-tunnel model, reference 19, were selected to show the anomalies found in the measured data, and how they developed as test conditions changed. This concept's wind-tunnel model and it's data was selected because there were no nacelle-wing reflection shocks in the flow field to confuse the identification of pressure signature features and sources.

Sketches of the B935 and the LB16 are found in Appendix C. A three-view sketch of the third concept, the HSCT-10B, is shown in figure 7.

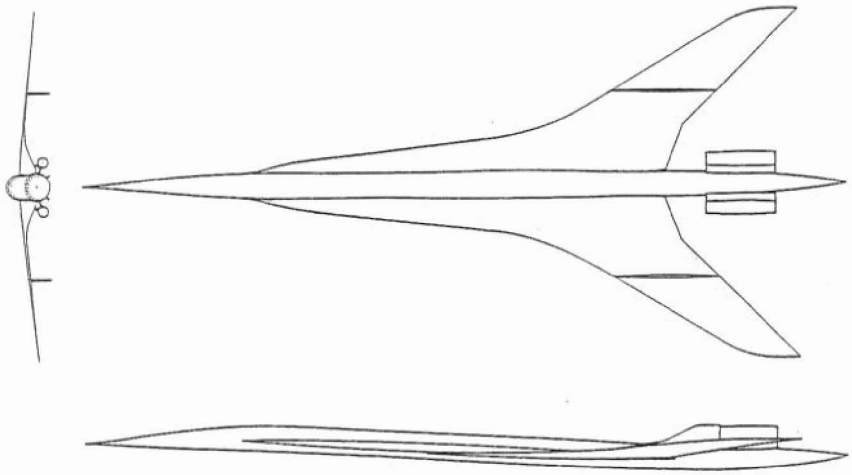

Figure 7. The Langley HSCT-10B conceptual aircraft.

The HSCT-10B wind-tunnel model had two sets of engine nacelles; each set sized for engines that would operate on different levels of propulsion technology. A schematic of these two types of nacelles are shown in Appendix D.

The HSCT-10B concept's volume and lift equivalent areas were tailored to produce a "low-ramp Hybrid" pressure signature and a ground overpressure of about 1.0 psf at start of cruise. Figure 8 shows a comparison of the ideal and predicted ground pressure signature.

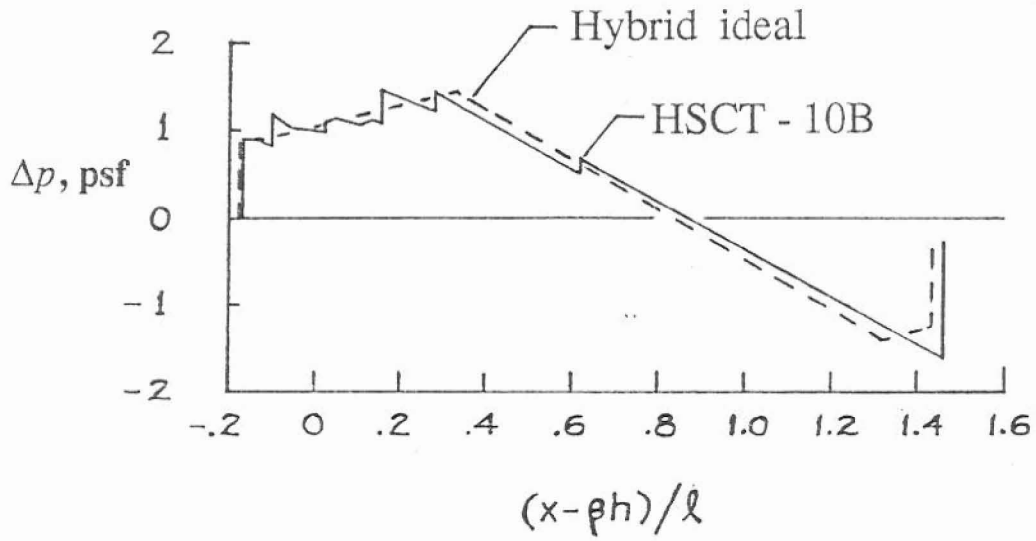

Figure 8. Comparisons of the ideal and the predicted HSCT-10B pressure signatures at start of cruise at M = 1.8 .

Wind-tunnel data, generated by the HSCT-10B wind-tunnel model at M =1.8, were recorded at a separation distance of 24 inches. Each set of nacelles was used to measure pressure signatures

with the model at $C_L = 0.0511$ ($C_L / C_{L,CRUISE} = 0.5$) and $C_L = 0.1022$ ($C_L / C_{L,CRUISE} = 1.0$).

The pressure signature measured with the *small* nacelles on the HSCT-10B wind-tunnel model at $C_L = 0.0511$ is shown in figure 9.

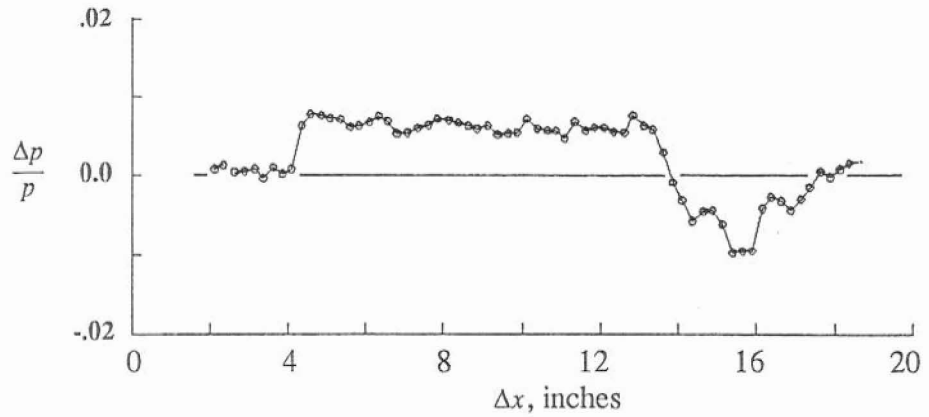

Figure 9. HSCT-10B model pressure signature. *Small* nacelles, M = 1.8, h = 24 inches, $C_L = 0.0511$, $C_L / C_{L,CRUISE} = 0.5$.

The pressure signature measured with the *large* nacelles on the model at $C_L = 0.0511$ is shown in figure 10.

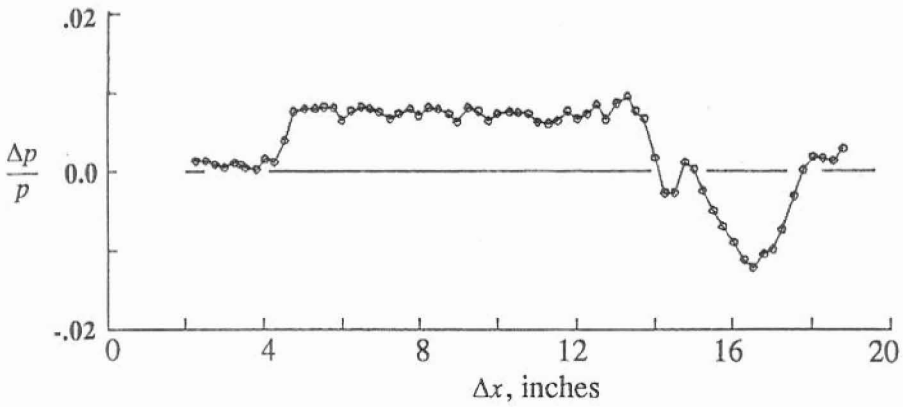

Figure 10. HSCT-10B model pressure signatures. *Large* nacelles, M = 1.8, h = 24 inches, $C_L = 0.0511$, $C_L / C_{L,CRUISE} = 0.5$.

Positive-pressure sections of the measured pressure signatures in figures 9 and 10 were almost identical in shape and length. Effects of the small and large nacelles were seen in the expansion-to-tail-shock part of the signature. The tops of the pressure signatures in figures 9 and 10 had virtually a "flattop" shape without indications of fuselage-strake, wing-fuselage, wing leading-edge crank, or nacelle shocks. However, the C_L of the wind-tunnel model generating these two pressure signatures was 0.0511, only half of $C_{L,CRUISE}$.

When the C_L on the model was increased to 0.1022, $C_L / C_{L,CRUISE} = 1.0$, the pressure signatures shown in figures 11 (small nacelles), and figure 12 (large nacelles), were measured.

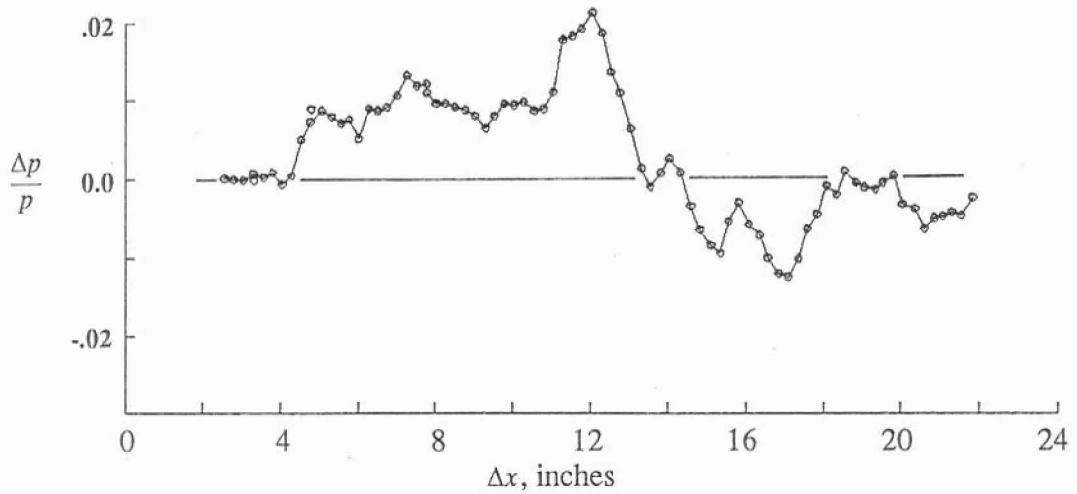

Figure 11. HSCT-10B model pressure signature. *Small* nacelles, M = 1.8, h = 24 inches, $C_L = 0.1022$, $C_L / C_{L,CRUISE} = 1.0$.

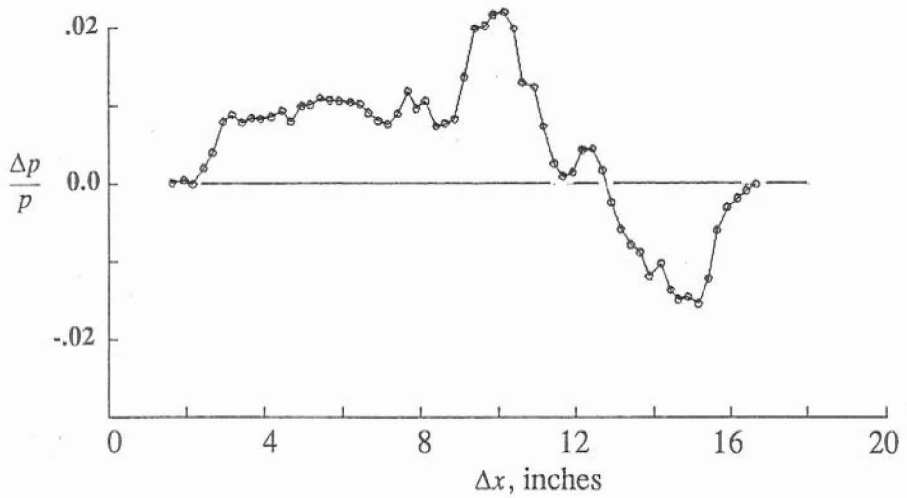

Figure 12. HSCT-10B model pressure signature. *Large* nacelles, M = 1.8, h = 24 inches, $C_L = 0.1022$, $C_L / C_{L,CRUISE} = 1.0$.

Again, the pressure signatures in figures 11 and 12 were similar in overall shape and length over the positive-pressure part. Small differences in the data points following the nose shock and preceding the wing-lift shock were random perturbations in the measurements. The strong shocks that appear prominently before the expansion to the tail shock system in figures 11 to 12 were due entirely to the increased wing lift (as $C_L / C_{L,CRUISE}$ increased from 0.5 to 1) that caused the almost-flattop-shaped pressure signatures in figures 9 and 10 to become the shock-dominated pressure signatures seen in figures 11 and 12.

This change in pressure signature shape was studied by measuring pressure signatures at two C_L ratios between $C_L / C_{L,CRUISE} = 0.5$ and $C_L / C_{L,CRUISE} = 1$. As the C_L of the model was increased in discrete steps, a gradual change in the model-generated pressure-signature shape could be seen that demonstrated the growth and cause of this pressure disturbance. This change in pressure signature shape, for the model with the large nacelles, is shown in figure 13.

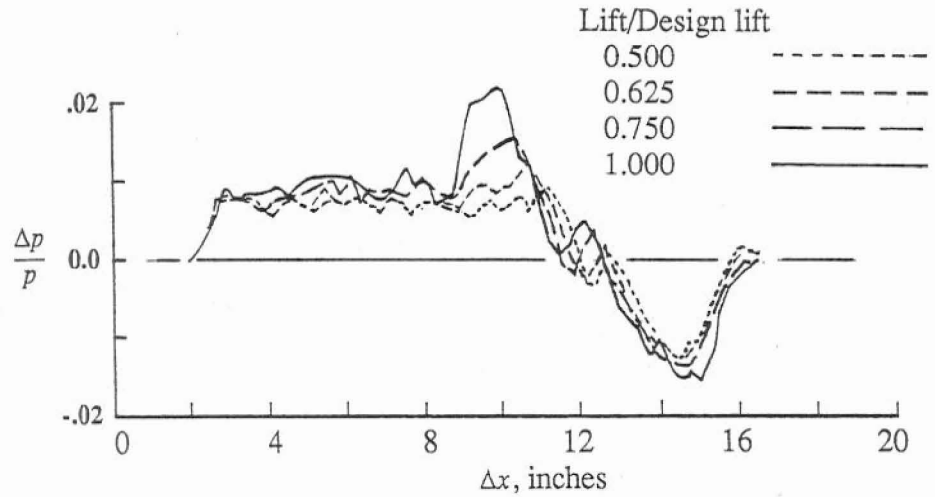

Figure 13. HSCT-10B model pressure signatures. Large nacelles, M = 1.8, h = 24 inches, with $C_L / C_{L,CRUISE}$ ratios of 0.50, 0.625, 0.75, and 1.0 .

The top of the pressure signature changed from almost "flat-top" to mild "ramp" plus a second shock over a C_L range where the $C_L / C_{L,CRUISE}$ ratio doubled. Ahead of the second shock, however, the slope of signature top was relatively gradual. This as well as the previous unexpected lift-induced shocks suggested other effects were present in near-field pressure signatures.

Langley Business Jet Concept And Model

After the HSR program ended, the focus of sonic-boom research turned from the HSCT to the Supersonic Business Jet (SBJ) sized aircraft. Less than half the length, and about a seventh the gross takeoff weight of the HSCT, the SBJ was expected to generate a pressure signature with a nose shock overpressure of only about 0.5 psf on the ground. The Concorde, designed with the mission performance technology of the 1960s, created a nose shock overpressure of about 2.0 psf, which was deemed objectionable to people on the ground in the flight "footprint". When the low-boom constrained HSCT was designed, an nose-shock overpressure of 1.0 psf was set as a limiting criteria, but even this nose-shock overpressure level produced noise and effects that were annoying to a significant fraction of the population. So the SBJ, low-boom tailored to generate a ground overpressure of 0.5 psf, seemed to be a supersonic-cruise vehicle whose nose shock overpressure would be within the "acceptance" (or tolerance) level.

Two sets of engine nacelles were designed for the Langley SBJ concept. One set, with small nacelles, was for high-performance, low-bypass-ratio engines. The other set, with large nacelles, was for high-bypass-ratio engines. A list of SBJ concept design and flight data is given in Appendix E.

Figure 14 shows a computer-generated three-view sketch of the Langley SBJ concept with the small set of nacelles.

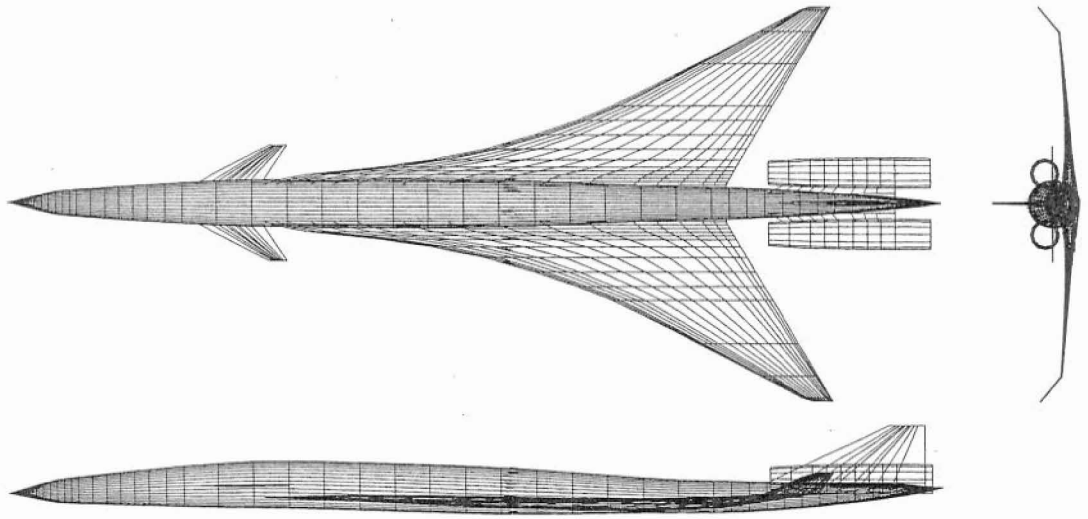

Figure 14. Langley Supersonic Business Jet Concept.

The SBJ concept's volume and lift equivalent areas were tailored to produce a "low-ramp Hybrid" pressure signature and a ground overpressure of about 0.5 psf. Figure 15 shows a comparison of the desired ground pressure signature with the pressure signature predicted from the configuration's volume and lift distributions at start of cruise.

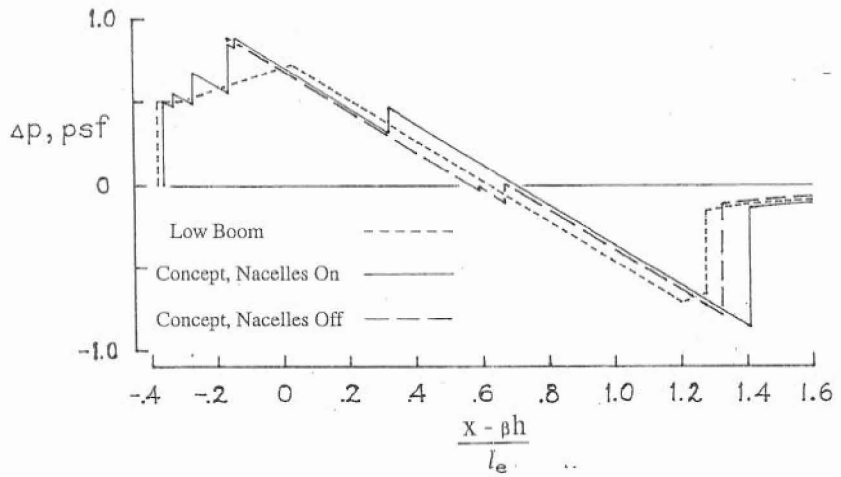

Figure 15. Comparison of desired and predicted ground pressure signatures.

The two pressure signatures in figure 15 show small nacelle disturbances in the expansion leading to the tail shock. These disturbances were of such low strength, relative to the nose and tail shocks, that they would probably be unnoticed by an observer on the ground.

However, the measured near-field pressure signatures generated by the model in the wind tunnel, reference 21, had anomalous shocks similar to those seen before. Three of these pressure signatures - the first of the configuration without nacelles, the second with small nacelles, and the third with large nacelles - are presented in figure 16.

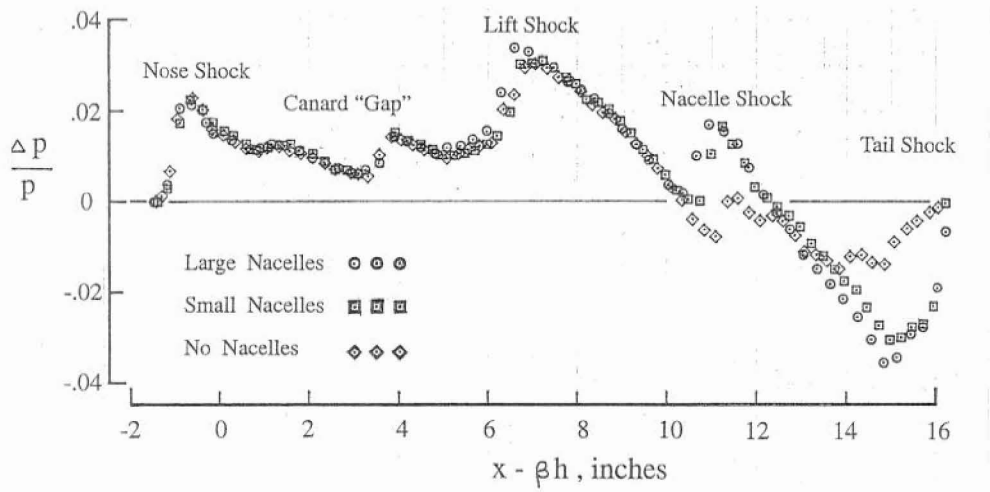

Figure 16. Measured pressure signatures from the SBJ model. $C_L / C_{L,CRUISE} = 1.0$, M = 2, and h = 18 inches.

The pressure signatures in figures 16 showed a very strong lift-induced shock preceding the expansion to the tail shock, just as was seen in the pressure signatures in figures 11 to 13. Since these lift-induced shocks appeared in the pressure signatures of HSCT and SBJ models, their appearance and evolution should have similar explanations.

There was a definite need to explain these anomalous shocks. Near-field wind-tunnel-measured pressure signatures are often extrapolated from cruise altitude to the ground (to obtain predictions of ground overpressures) with the Thomas Extrapolation Code, reference 26. This code is based on a first-order, two-dimensional, cylindrical propagation model, as is the propagation model in Whitham Theory. It is used even though there is a physical mismatch in the two flow fields around and along the line of application. When near-field pressure signatures, like those shown in figure 11, 12, 13, and 16 are extrapolated to the ground, a distorted low-boom or an N-wave pressure signature with $\Delta p > 0.5$ psf, rather than a low-boom-shaped pressure signature with $\Delta p = 0.5$ psf, could very likely be predicted. Since near-field pressure signature extrapolation is done in spite of its inherent physical shortcomings, it is important to determine the cause of these anomalous shocks, how far into the flow field they will persist, and what strength they might have if the extrapolation was performed properly.

Possible Causes Of Anomalous Shocks

In the previous sections, nacelle volume and nacelle-wing interference lift were identified as one cause of anomalous shocks on measured pressure signatures from low-boom wind-tunnel models. Yet, there were other unexpected lift-induced shocks on measured pressure signatures that required an explanation. Some were due to the linearized-theory method, reference 27, for calculating the wing lift and the area-ruled lift distribution. That particular wing performance computer code was modified and updated to account for theoretical non-linearities. It became the replacement, reference 22, for the lift-analysis code used to design supersonic-cruise as well as low-boom concepts. Still, this singular hypothesis did not explain all the lift-induced shocks that continued to appear in measured near-field wind-tunnel pressure signatures. The measured

pressure signatures presented in references 19 and 21 demonstrated the anomalous shocks were still present even though the more-exact method of reference 22 had been employed to calculate the area-ruled lift equivalent areas. Research suggested that near-field effects might also be a cause. These near-field effects were the basis of a suggestion in reference 24 that the Thomas Code was being applied to pressure signatures measured at too close a separation distance. Now, near-field effects were re-examined as a possible cause of anomalous shocks.

A third possible cause of anomalous shocks was concerned with the accuracy of the longitudinal area-ruled lift distributions due to inaccurate calculation of surface pressures along the outer panels of highly-tapered wings used on supersonic-cruise concepts. In the next sections, these second and third hypotheses will be discussed and evaluated.

Near-Field Effects

The near-field effects being analyzed were due to the close proximity of the survey probe to the lifting wing-body model, not to the nonlinearity of shocks. They would probably be most noticeable directly below the flight track. There, volume effects added to the lift effects where the lift effects were maximum. Three theoretical flow-field models were employed to identify these effects and determine their magnitudes. The first model was a flat lifting delta wing. It was used to determine the different areas of lift influence at near- and far-field conditions. The second and third models were a slender delta wing and a slender cone, represented by a line of doublets and a line of sources respectively. The ratio of the impulse from these two models was calculated at different Mach numbers and at increasing separation distances.

Delta-Wing in Supersonic Flow

Consider a delta wing model with a subsonic leading edge, $\beta \cot \Lambda < 1.0$, cruising supersonically at a very small angle of attack; like the delta-wing model shown in figure 17.

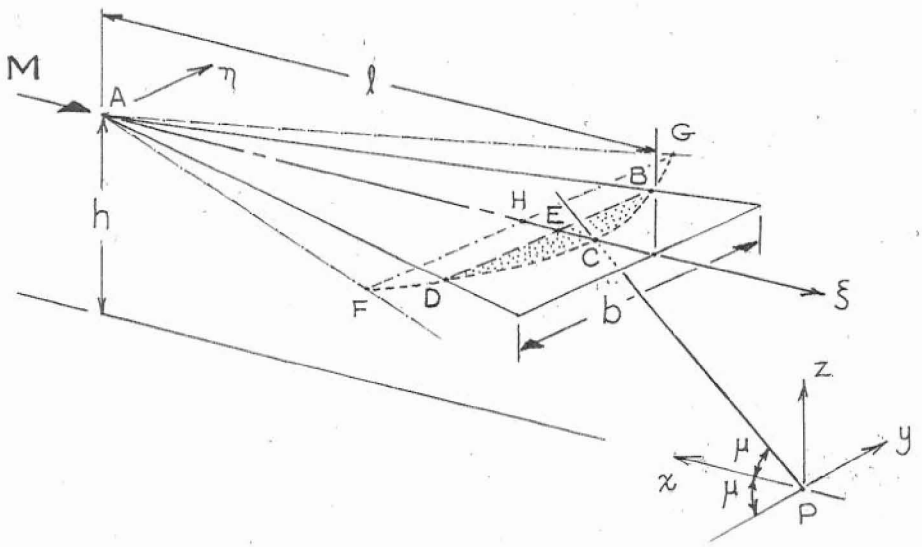

Figure 17. Simple slender delta wing in supersonic flow.

For clarity, camber, twist, and airfoil thickness have been omitted, leaving a flat delta surface for evaluating the wing areas that influence the field pressure at point P. These areas are confined by a Mach cone from point P and the flow field that intersects the wing surface with its apex-cen-

tered shock conoid. For convenience, this apex shock conoid is approximated by a Mach cone whose intersection with the Mach cone from point P in the plane of the wing is $AGBCDF$.

Three assumptions were used in this model and derivation: (1) lower surface pressures were more influential than upper surface pressures; (2) lift effects extended from the wing leading edge to the shock; and (3) lifting pressures were almost uniform. If wing leading edge was subsonic, the leading edge upwash influences could be strong and would add to the lifting pressures along the leading edge. However, they would decrease in strength between the leading edge and the shock originating at the wing apex or the vehicle's nose. So, the model would be useful at and near the design Mach number, but had to be used with caution when the leading edge flow was supersonic or when the Mach number was much less than the design Mach number.

Wing / Shock Intersections

A measure of the near-field lift influences reaching point P and the far-field lift influences reaching point P could be represented with the areas $ABCD$ and $ABED$ respectively. The line EC would be a simple, direct, way of representing this difference in the near-field and far-field effects on the wing. Flow field influences would also come from ahead of the lifting surfaces if the wing had a subsonic leading edge. To include these extra influences, the Mach cone at point P was extended beyond the wing leading edges to the shock cone (represented by a Mach cone) whose vertex was at the wing apex so that the extended wing plane, the delta-wing apex shock, and the Mach cone anchored at P intersected at points F and G. A Mach cone anchored in the far field would intersect along FHG, while the near-field Mach cone would intersect along $FDCBG$. So now, the line HC, instead of EC, would represent the difference between near-field and far-field influence areas. Along the plane of symmetry where $y = 0.0$, the longitudinal component of the distance between field point P and wing-surface point C would be:

$$\beta h$$

At point G, the wing-apex centered Mach cone is intersected by the wing-plane line HG which runs parallel with the y- axis. The longitudinal distance from point P along the x-axis to point G, the apex Mach cone / wing-plane line intersection, would be:

$$\sqrt{(\beta h)^2 + \left(\frac{FG}{2}\right)^2}$$

The difference, HC, could be designated either Δx or $\Delta\xi$ because the x-axis and wing reference line along ξ were parallel. This incremental length was:

$$\Delta\xi = \Delta x = \sqrt{(\beta h)^2 + \left(\frac{FG}{2}\right)^2} - \beta h$$

The right hand side of the equation was expanded in a series. $\Delta\xi$ was made dimensionless with the local span, $b(\xi) = DEB$, which was coincident with the far-field cone intersection. Then, the length ratio, HC / BD, could be approximated by the first term of that series:

$$\frac{HC}{BD} = \frac{\Delta\xi}{b(\xi)} \approx \frac{1}{8\beta\left[\frac{h}{b(\xi)}\right](\beta\cot\Lambda)^2} \qquad (1)$$

where Mach number and the wing geometry effects are represented by the terms β and $\beta\cot\Lambda$. A similar equation, where the field point Mach cone intersected with the wing leading edge, was derived in reference 24, and could be obtained from equation (1) by setting $\beta\cot\Lambda = 1.0$.

The ratio $\Delta\xi / b(\xi)$ could be calculated for any value of h/b, but results from h/b values

less than about 0.50 would not be very accurate because equation (1) has only the first term of a truncated series. However, values of $\Delta\xi / b(\xi)$ obtained from small h/b values could be used to determine relative near-to- far-field influence effects. Most supersonic-cruise concepts have wing lift l/b ratios in the range of 1.5 to 2 . They usually cruise at low α with $C_{L,CRUISE}$ close to 0.10. So, very low values of $\beta \cot \Lambda$, either because of low Mach numbers or high wing leading edge sweep angles, are inappropriate except when studying local lift effects along highly-swept strakes between the wing apex and the wing tip.

Using equation (1) to demonstrate near-field flow effects, values of $\Delta\xi / b(\xi)$ were calculated with $b(\xi)$ set equal to the span of the delta wing at the trailing edge. This ratio was plotted versus h/b for three different values of $\beta \cot \Lambda$ in figure 18.

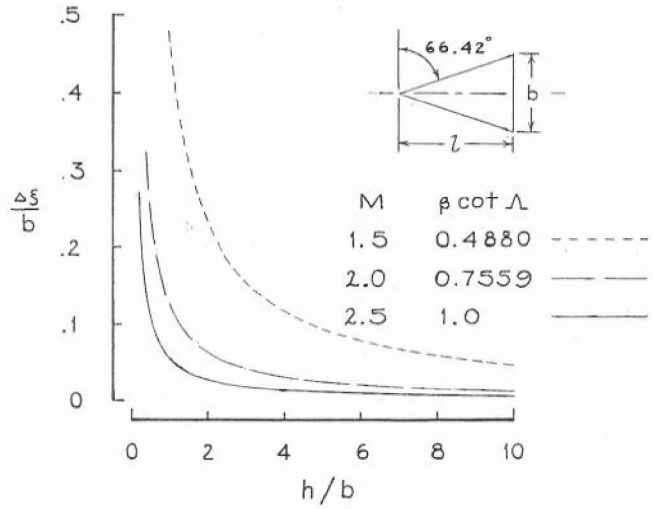

Figure 18. ξ / b versus h/b for a sample delta wing at Mach numbers of 1.5, 2.0 and 2.5.

The local curvature of the wing-intersecting Mach cone (with vertex at flow-field point *P*) rapidly "flattened" with increasing h/b, and approached far-field "planar" area-ruling conditions. As the Mach number increased, this far-field "planar" condition occurred at a vertical distance closer to the wing. This was the result of the Mach cone angle becoming narrower with increasing Mach number, which forced the flow-field point P to be located farther behind the wing.

Upper-wing lift disturbances felt in the flow field at point P would come from the surface area forward of, and less than, area *ABED*, while all lower-wing surface lift disturbances would come from the surface area *ABCD*. The flow-field areas *ABG* and *ADF* were avenues through which the upper-wing disturbances would propagate into the flow field around the wing. Since the lower-wing areas were larger than the upper-wing areas, and were closer to the field point P (survey probe in wind-tunnel tests), the lower-wing surface lift would be much more influential than the upper-surface lift, and its vectored effect could be the source of unexpected disturbances or shocks in the near-field pressure signature produced by a low-boom tailored configuration. This hypothesis was explored further in the *Impulse Comparison* section.

The wing lift usually begins well aft of the nose on a low-boom concept or model so that forebody volume can grow as rapidly as possible. Since the wing contributes to the volume behind the nose shock, the span becomes an important parameter as the Mach number changes. The wing planform on a low-boom configuration is seldom a simple delta, but is more likely a long modified-arrow wing. By considering this configuration's wing to be composed of a large number

of smoothly merged delta wings, the local near-field effects can be estimated. Thus, equation (1) could be a useful geometry-based indicator for evaluating the extent of near-field effects, due to wing lift, on a delta-wing/body model's wind-tunnel pressure signature.

In the "far-field", *EC* and *HC* would be approximately zero, and the points *FDCBG* would be approximately coincident with points *FDEBG* to form an almost-straight line. Upper-surface pressure influences would merge with lower-surface pressure influences, and be felt at P, now at a very large distance h below the wing as originating from a body of revolution. Since the lift distribution used in low-boom tailoring of conceptual aircraft was based on these far-field considerations, i.e. the Mach-plane-sliced lift distribution, pressure signatures measured in the very near field could show increased lower-wing influences as lift-induced shocks. These lift-induced shocks would likely originate from regions where the wing leading-edge sweep angle, the wing area, and/or and local lift gradients, were increasing rapidly.

Impulse Comparison

The pressure signature impulse, maximum positive value of the integral of the pressure disturbances, from either a body of revolution or a lifting wing body (both with equal equivalent areas) would be equal in the far field. In the near field, however, the magnitudes of these impulse values would be considerably different, as would be the shapes of the pressure signatures and the relative strengths of their volume and/or lift generated pressure disturbances.

A line of doublets was used to represent the lift-generated disturbances from a slender wing at small angle of attack[1]. This simplified cross-flow model, similar to and representing the lift on a slender delta wing, emphasized the effect of lifting length over the effect of span. For comparison, a line of sources, representing a slender conical body-of-revolution at zero angle of attack, was used to generate volume-induced disturbances. The cone had a maximum cross-section area equal to the far-field equivalent area due to lift of the slender delta wing. These models made it possible to compare lift and volume disturbances (via their impulse) under both bodies with increasing separation distances.

Since only the effects of volume and lifting length were studied in this comparison, the cone length was set equal to the wing lifting length. The two disturbance-generating "bodies" were much too slender to generate finite-strength near-field nose and trailing shocks. Thus, the impulse, I, instead of shock strength, was used as a measure of the flow-field disturbance generated by both the slender cone and the slender delta wing in supersonic cruise flight.

The impulse from either the slender delta or the slender cone can be written as:

$$I = [\gamma p M^2 \int (-u)dx]_{MAX} \quad \text{or} \quad I = [\int (\Delta p)dx]_{MAX} \tag{2}$$

since, in slender-body theory

$$\Delta p \approx -\gamma p u M^2 \tag{3}$$

where u is defined as the nondimensional longitudinal perturbation velocity.

The longitudinal perturbation velocity generated by a slender cone, u_c, can be defined as:

$$u_c = -\frac{A_{e,c}}{2\pi} ln[1.0 + \zeta + \sqrt{\zeta^2 + 2\zeta}] \tag{4a}$$

1. Suggested by Harry W. Carlson; NASA Langley Research Center, retired

where

$$\zeta = \frac{x - \beta h}{\beta h} \; ; \quad x > \beta h \tag{4b}$$

Slender delta wing lift develops longitudinally very much like the cross-sectional area of a slender cone. Using cross-flow theory for flow around very slender delta wing at low angles of attack, the longitudinal perturbation velocity, u_w , is derived as:

$$u_w = \frac{A_{e,w}\beta \sin\alpha \cos\theta}{\pi} \sqrt{\zeta^2 + 2\zeta} \tag{5a}$$

Under the flight path, $\theta = 180.0$,degrees, so:

$$u_w = \left(-\frac{A_{e,w}\beta \sin\alpha}{\pi} \right) \sqrt{\zeta^2 + 2\zeta} \tag{5b}$$

where, in agreement with the far-field results of reference 12,

$$A_{e,c} = 2\beta A_{e,w} \sin\alpha \tag{6}$$

and $A_{e,c}$ is determined from the source strength distribution of the slender cone. Once $A_{e,c}$ was calculated, the flight Mach number and the angle of attack permitted $A_{e,w}$ to be found.

Impulse could also be obtained from an integration of the Whitham F-function, if this was used to calculate u_c or u_w . Since slender-body and cross-flow theories were employed, the perturbation velocity, u , in equations (2) and (3), was equal to either u_c or u_w , the perturbation velocities defined by equations (4a) or (5b).

The ratio of the slender delta-wing lift impulse to the slender-cone volume impulse, I_w / I_c , as a function of the distance ratio, h / l , was numerically calculated from equations (4) to (6) at Mach numbers of 1.6, 2.0, and 2.4 . Since the flow-field overpressures were integrated along the length of both the slender delta and the slender cone, the length rather than the span appeared in the results presented in figure 19.

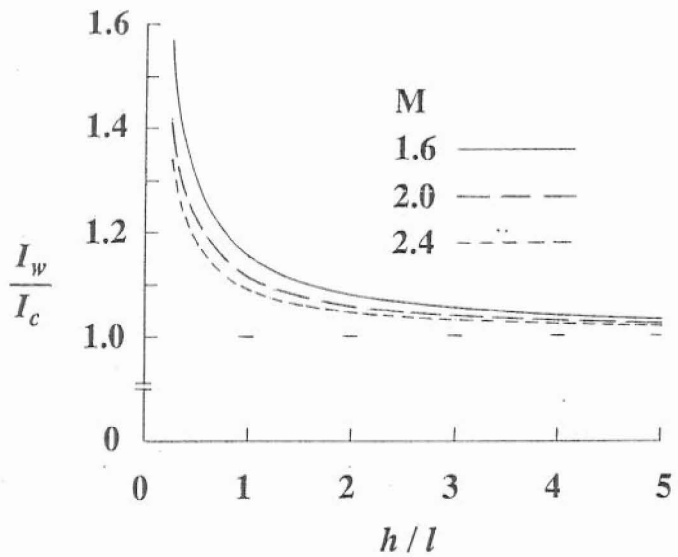

Figure 19. Ratio of impulse, I_w / I_c , from slender delta-wing lift and slender cone volume versus h / l.

The impulse curves presented in figure 19 showed that lift-generated impulse could be considerably larger than volume-generated impulse in the near field. Individual overpressures in the measured pressure signature would also show the same effect. With increasing h/l, the impulse ratio, I_w/I_c, would approach the far-field value of unity given by Walkden in reference 12, and set by the boundary conditions in equation (6). The effect of Mach number on I_w/I_c was similar; noticeable at low Mach number, and diminishing as Mach number increased.

These flow-field models, the physics of near-field/far-field influence equations, and the interpretation of the numerical results strongly suggested that near-field effects could be the cause of, or contribute to the appearance of, anomalous shocks in the measured pressure signatures of lifting low-boom models at h/l values of 5 or less. There would be a Mach number dependence, and for a wing/fuselage/nacelle/fin concept, a dependence on the ratio of lift equivalent area to volume equivalent area as well. In spite of all efforts to tailor the volume and lift for a low-boom pressure signature shape on the ground, the close proximity of the model and the survey probes could result in higher lower surface pressures exerting unduly-high influences on the overpressures being measured by the survey probes. However, there were other possibilities, and these are discussed in the following sections.

Theoretical Lift Distributions

A third possible cause of anomalous shocks was mentioned and discussed in a private communication[2]. It was noted that while the Modified Linear Theory Method, reference 22, was a marked improvement over the Linearized Theory method, reference 27, it did not always accurately predict the lifting pressures on the upper and lower surfaces of the outer wing panels of some wings.

On a low-boom model wing, with the Modified Linear Theory Method code used to analyze and to tailor a minimum-drag camber surface, the outer wing panels might be credited with providing more lift than they were actually generating. If the outer panels were generating less lift than predicted, the usual situation, an extra increment in angle of attack would be necessary to bring the lift up to the desired level during flight or wind-tunnel tests because the inner panels would have to provide the lift not developed by the outer panels. Now, the longitudinal lift gradients would be higher than designed, because the inner-panel lift would grow faster and reach higher levels. When the overpredicted surface pressures covered a significant percentage of the outer wing panels, and/or the magnitudes of the overpredictions were large enough, these errors in local lift estimation could enhance the possibilities of unexpected lift-induced shocks appearing in the near-field and cruise-field pressure signatures.

The question of accurate surface pressure prediction was addressed in reference 29. A computer code called *EMTAC* (Euler Marching Technique for Accurate Computation) was used to predict surface pressures on some research arrow wing models. Surface pressures predicted by *EMTAC* were compared with the surface pressures measured on the three arrow-wing models that had been described, analyzed, and discussed in reference 30. Euler code predictions of surface pressures at all the specified semi-span stations, but especially at the outer wing stations, were in better agreement with the measured surface pressures than were those from the Modified Linear Theory Method code at the angles of attack associated with HSCT or SBJ cruise flight. These comparisons, from the Euler code and references 22 and 29 are shown in figure 20.

2. Eric Adamson, Boeing Aircraft Company

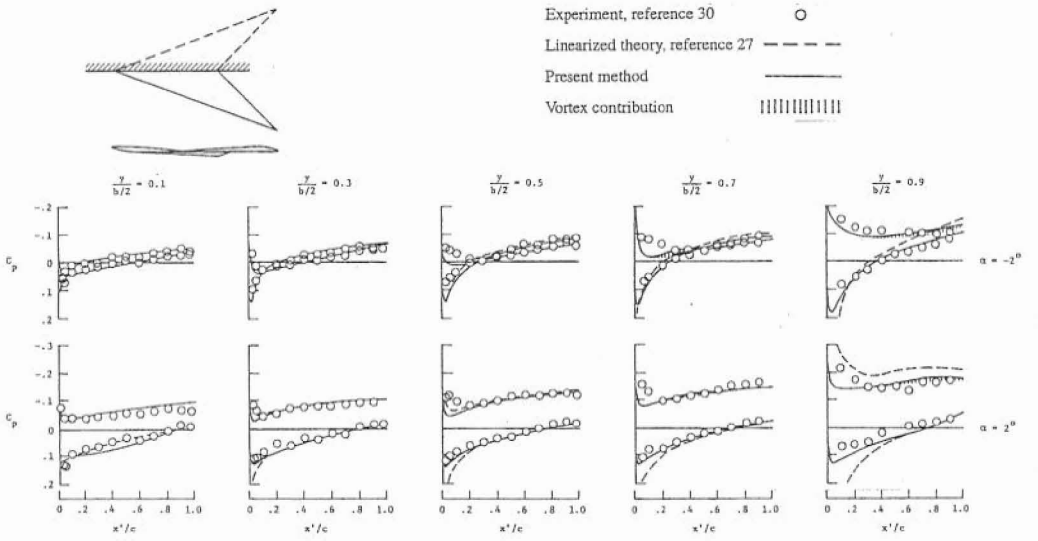

(a) Reference 27, Linear theory

Figure 20. Sample comparisons of theory and experiment. Arrow wing, reference 30, designed for $C_{L,CRUISE} = 0.08$.

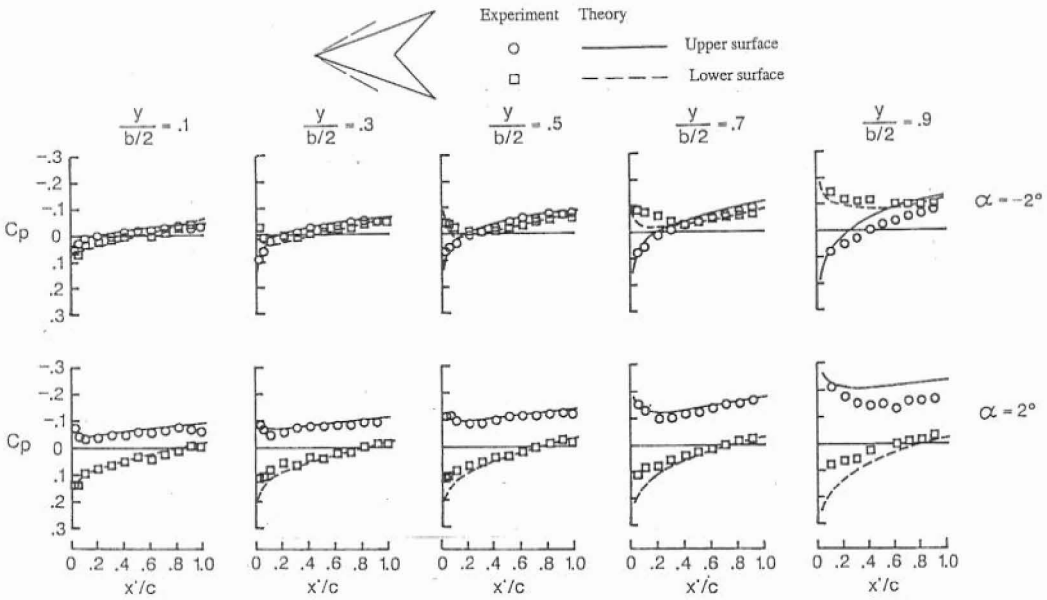

(b) Reference 22, Linear and Modified Linear theory

Figure 20. Continued

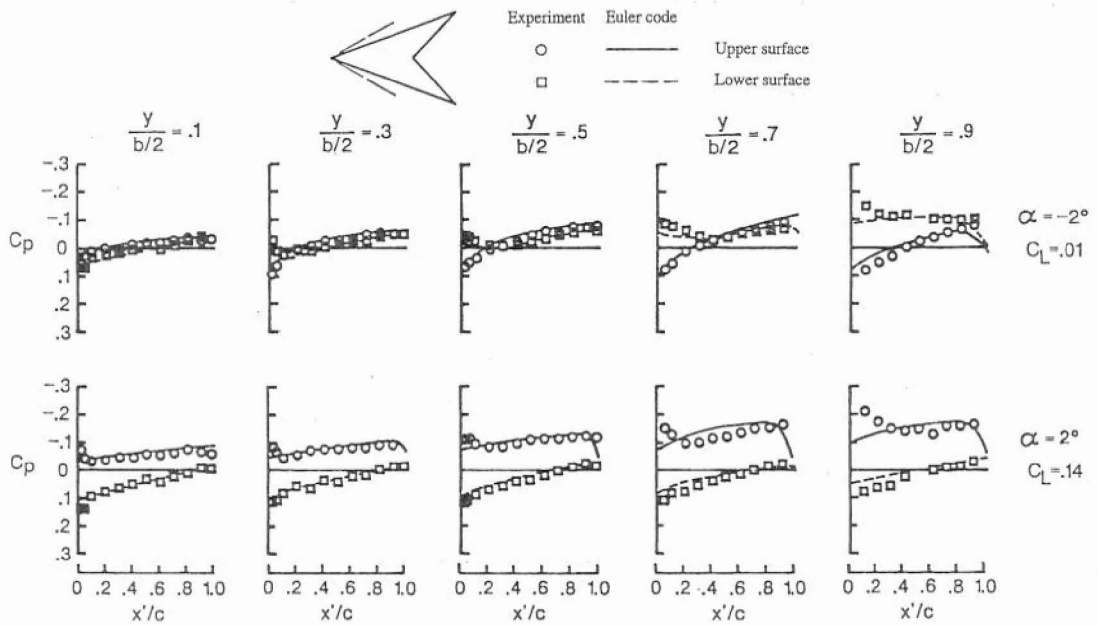

(c) Reference 29, Euler code.

Figure 20. Concluded

Experimental data in references 22 and 29, figure 20, indicated the communicated observation was correct for some of the wing models in the study. The accuracy of the aerodynamic force data might not suffer appreciably, but the tailoring of the configuration's lift for low-boom might be compromised, depending on the ratio of outer-wing panel lift to total wing lift. If small, this effect might be seen in the near field pressure signature with the appearance of a noticeable change in signature shape on the positive pressure section of the pressure signature immediately preceded the expansion to the tail shock. It would add to any near-field effects already present in the model's overpressure field. A serious outer wing panel lift underprediction could result in a strong perturbation or shock in the near-field pressure signature that could coalesce with, and strengthen, the nose shock after it propagated through the atmosphere to the ground.

Scale Effects

A fourth possible cause of unexpected shocks was also mentioned and discussed in the aforementioned communication[3]. It was related to the third cause - the loss of expected lift on the outboard wing panels. In this case, however, the possible cause was tip stall due to the small size of the sonic-boom models. Now, the loss in prediction method accuracy would be due to separated flow, but the same inaccurate prediction of surface pressure result might be seen in the measured pressure signatures. Similar to the lack of computational lift-prediction accuracy previously mentioned, the loss of lift on the tip panels would force the inner wing panels to make up the difference in lift, so that $C_{L,CRUISE}$ would be maintained during the measurement of the pressure signature. More angle of attack would then be required to maintain this desired $C_{L,CRUISE}$ which

3. Eric Adamson, Boeing Aircraft Company

would decrease the effective length of the model, increase the longitudinal lift gradients, and enhance the possibilities of local pressure disturbances becoming shocks. The effect might not be noticed when pressure signatures were measured at $C_L / C_{L,CRUISE} = 0.5$, figures 9 and 10, but could be noticeable when pressure signatures were measured at $C_L / C_{L,CRUISE} = 1.0$. Thus, the measured pressure signatures of the HSCT-10B model at the in-between $C_L / C_{L,CRUISE}$ ratios, figure 13, and the SBJ model, figure 16, could be explained by either a gradual onset of tip stall, by near-field effects, or a combination of both.

The wind-tunnel model wing tip chords on the HSCT-10B model were found to be longer than those on the SBJ by a factor of two. A second factor, the required angle of attack of the SBJ model at $C_L / C_{L,CRUISE} = 1.0$, was about 50 percent higher than that on the HSCT. There was also a third factor: the wing tip twist on the HSCT-10B, which was higher than the wing tip twist on the SBJ model. While these three factors - tip chord length, angle of attack, and tip twist - strongly suggested that wing-tip stall might a cause of the lift-induced shock on the SBJ model, and that near-field effects were probably the cause of lift induced shock on the HSCT-10B model, no well-documented conclusions could be made on the basis of pressure signatures from only two models and the small number of measured pressure signatures. Perhaps, photographic surface flow studies done by applying fluorescent dyes in oil to the model's surface, and more pressure signature measurements made at varying angles of attack could be used to answer questions of which effect(s), and its/their magnitude(s), was/were present.

Analysis and Discussion

Near-Field Effects

Near-field effects, derived in the previous sections, could be a cause, but not the only cause, of anomalous shocks appearing behind the nose shock on the positive section of the pressure signature. One of the near-field effects was due to the higher lower wing surface lifting pressures being closer to the survey probe(s), thus exerting more influence on the survey probe than the upper wing surface lifting pressures at a farther distance.

The second effect was due to the lift-generating wing acting like a dipole, directing flow downward rather than radially outward like a source. These momentum effects exaggerated the influence of the lift gradients in the air directed downward by the lift-producing wing, and carried through the flow field to the probe(s). Such near-field effects tended to increase the strength of the pressure disturbances in the flow field under the wind-tunnel model, and could promote the formation of extra near-field shocks not predicted by the application of the sonic-boom minimization theory method based on far-field models and assumptions. Whitham theory, also based on far-field assumptions, could accurately predict the shape of the forward section of the pressure signature if volume disturbances were the only ones present in the flow around the fuselage forebody. However, Computational Fluid Dynamic (CFD) codes would be capable of calculating the strength and location not only of these volume-induced shocks and overpressures, but of predicting the entire near-field pressure signature caused by volume, lift, and mutual interference contributions.

Since near-field effects have been identified as a possible source of anomalous near-field shocks, then there should be a practical "transition" separation distance. At this "transition" distance, the near-field effect of meridian pressure gradients would have diminished to the point where, for practical extrapolation purposes, they were at least a magnitude or two smaller than the

two-dimensional attenuation effects (longitudinal spreading and radial weakening) occurring at the same time in the flow field. This question could also be restated as: At what separation distance would these near-field anomalous shocks disappear by attenuation and merge with the other overpressures in the positive part of a shaped low-boom signature?

In reference 24, the ratio

$$\frac{\Delta x}{Mb} \approx 0.01 \tag{7}$$

was suggested as a conservative measure of certainty that anomalous shocks had attenuated and disappeared into the top of a low-boom shaped pressure signature before they would coalesce with, and strengthen, the nose shock; or that "quasi-two-dimensional-flow field" conditions had become established so that pressure signatures could be extrapolated with the Thomas Code. Since equation (1) already contained a Mach number factor, the ratio

$$\frac{\Delta \xi}{b} \approx 0.01 \tag{8}$$

was used instead. It was assumed, for this exploratory calculation, that $\beta \cot \Lambda = 0.8$ was a reasonable wing leading edge sweep parameter at Mach 2. Then, from equation (1):

$$\frac{h}{b} \approx 11.3 \tag{9}$$

This separation distance would be difficult to obtain in a 4 ft x 4 ft wind tunnel test section, such as the one in the Langley Unitary Plan Wind Tunnel Facility, unless the wind-tunnel model had a span of about 2.5 inches and a length of about 5.0 inches. If the model had a span of about 6.0 inches and a length of 12 inches, a larger wind-tunnel test section, such as the 10 ft x 10 ft Supersonic Wind Tunnel Facility test section at the John Glenn Research Center, would provide the required volume to measure pressure signatures at separation distance to span ratios that achieved, or even exceeded, the h/b value designated in equation (9).

A parallel impulse calculation was performed with the equations used to obtain the data in figure 19. An impulse ratio corresponding to the constraint in equation (8) was used to calculate an h/l value similar to the result in equation (9). This impulse constraint would be:

$$\frac{I_w}{I_c} \approx 1.01 \tag{10}$$

At a Mach number of 2.0, the calculated value of:

$$\frac{h}{l} \approx 11.5 \tag{11}$$

corresponded to this impulse ratio. Although the values in equation (9) and (11) were numerically close, no analytic correspondence between the span, b, and the length, l, exists in this general analytical model because the slender cone and the slender delta wing impulse was derived from slender-body cross-flow theory. The value of h/b in equation (9), calculated from the constraint given in equation (8), was obtained from an acoustic model of a delta wing and its flow field, while the value of h/l in equation (11), calculated from the constraint in equation (10), was obtained from the integral of the overpressures generated in the flow field. Nevertheless, h/b versus Mach number and leading edge sweep angle was calculated from equation (1), and plotted along with an h/l versus Mach number calculated with equations (4) to (6). These curves permitted qualitative comparisons of trends to be made with the Mach number as the common

parameter. The results of these calculations are shown in figure 21.

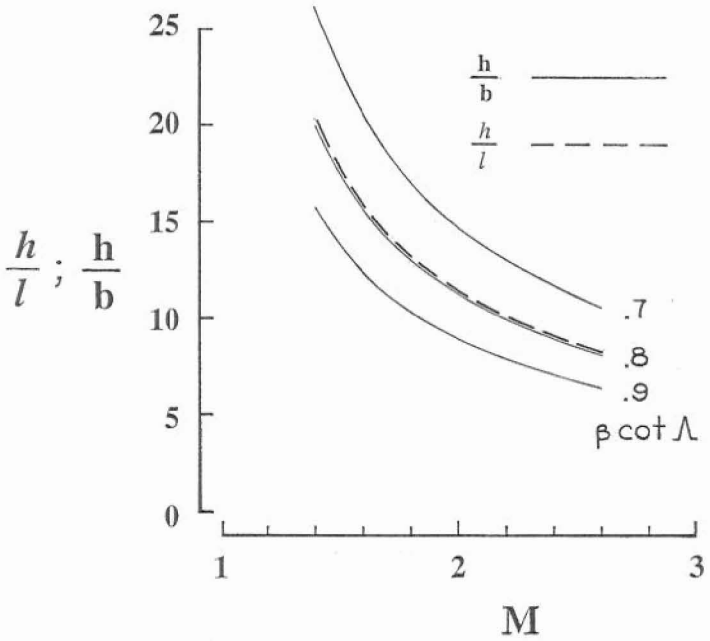

Figure 21. Transition h/b with $\Delta\xi/b = 0.01$ for delta-wing $\beta \cot \Lambda$ of 0.7, 0.8, and 0.9; transition h/l with $l_w/l_c = 1.01$; Mach No. = 1.4 to 2.6 .

Transition values of h/b calculated with equation (1) for the slender delta wing decreased with increasing leading edge sweep angle and increasing Mach number. Similarly, transition values of h/l calculated with equations (2) to (6) for the slender cone decreased with increasing Mach number. All the theory curves for transition values of h/b and h/l had virtually the same shape and followed the same trends as Mach number increased.

Since shocks are a localized feature, the pressure gradients due to leading edge sweep that could provoke the shocks are important factors in determining where a low-boom pressure signature would transition from a near-field shape to a "limiting distance" shape. Therefore, equation (1) might be a somewhat better indicator of "transition distance" than the impulse for an SBJ concept, although the impulse could be used as a corroborative indicator. If the concept was the size of an HSCT, where the equivalent areas due to lift were considerably larger than those due to volume, the impulse might prove be the better indicator.

These ideas were tested by first using h/b as the comparison parameter with $\Delta\xi/b$ as a "transition indicator". The value, $\Delta\xi/b = 0.01$, was used in equation (1) and applied to the wind-tunnel models discussed in the section *Pressure Signatures* to obtain estimates of h/b (transition). This value, obtained from equation (1), was designated:

$$\left(\frac{h}{b}\right)_1 = \frac{h}{b} \tag{11}$$

Then, equation (2) to(6) were used to obtain a value of h/l for the same wind-tunnel models discussed. The calculated value of h/l for the appropriate Mach number was converted to an h/b value by multiplying the value of h/l by an appropriate value of l/b for each particular wind tunnel model. Using this empirical device, both length and span were brought together to create a concept-specific impulse parameter. This second h/b value was designated:

$$\left(\frac{h}{b}\right)_2 = \left(\frac{h}{l}\right)\left(\frac{l}{b}\right) \tag{12}$$

where the parameter, l, was the lifting length, rather than the overall or effective length, of the particular concept or model.

All of these concepts were flying wing configurations. Their wings had curved leading edges and some form of a modified ogive-arrow planform with a rounded apex. So, a "mean" or "representative" delta wing was obtained by employing an area-span "averaging" method. The value of the leading edge sweep parameter, $\beta \cot \Lambda$, on the wings of the concepts used as examples was between 0.70 and 0.90 at the cruise Mach number. Rounded-off results obtained from equations (11) and (12) are listed in Table I, with h designated, as before, as the distance directly below the flight track.

Table I. Estimated values of h/b (transition) for research concepts and wind-tunnel models.

Concept	Mach No.	$(h/b)_1$	$(h/b)_2$
Mach 2	2.0	13	22
Mach 3	3.0	6	15
HSCT-10B	1.8	13	21
Langley SBJ	2.0	10	18

None of the empirical values of $(h/b)_1$ and $(h/b)_2$ were in close agreement. The $(h/b)_1$ results emphasized the effects of span with the length of the representative delta wing adjusted to keep the areas constant, while the $(h/b)_2$ results emphasized the effects of the lifting length, with both the length and the span equal to those on the particular concept. This emphasis on impulse and lifting length resulted in the $(h/b)_2$ results always being larger by about 50 percent, and made them the much more conservative estimates of transition distance.

If the wing had a swept trailing edge (an arrow wing), the leading edge sweep and the $(h/b)_1$ value would be larger for the same area and span. Adjusted values of $(h/b)_1$, called $(h/b)_{1,\,ADJ.}$, were calculated, and with the previous values of $(h/b)_2$, were listed in Table II .

Table II. Adjusted values of h/b (transition) for research concepts and wind-tunnel models.

Concept	Mach No.	$(h/b)_{1,\,ADJ.}$	$(h/b)_2$
Mach 2	2.0	15	22
Mach 3	3.0	7	15
HSCT-10B	1.8	23	21
Langley SBJ	2.0	16	18

Adjusted $(h/b)_1$ values in Table II, $(h/b)_{1,ADJ.}$, were larger than the $(h/b)_1$ values in Table I. except for the $(h/b)_1$ value of the Mach 3 concept, whose wings had very little trailing edge sweep. These adjusted $(h/b)_1$ values agreed better with $(h/b)_2$ values already calculated. The unusually large increases in $(h/b)_{1,ADJ.}$ values on the HSCT-10B and Langley SBJ concepts were due to the high trailing edge sweep on their wing planforms. Except for those of the HSCT-10B, the $(h/b)_2$ values were the larger and more conservative estimates of transition distance ratio. Thus, for this small sample of supersonic-cruise concepts and their wind-tunnel models, wing

planform shape - leading and trailing edge sweep angles - seemed to be as significant as the ratio of lift to volume equivalent areas.

The values of $(h/b)_1$ and $(h/b)_2$ for the Mach 3 concept demonstrated the effects of higher Mach numbers. Although the radial distance, h, was small, the longitudinal distance was larger by a factor of the Mach number parameter β. So, while it might be easier to obtain this shorter separation distance in the cross section of a modest sized wind-tunnel test section, the length of the test section required to obtain a complete pressure signature might prohibit measuring a complete pressure signature at this separation distance. Another consideration is that Seebass and George Minimization Theory is based on Whitham theory which starts to lose its accuracy and applicability at Mach numbers above 2.5 .

If the average or the numerical mean of the two values were used, a bit more optimistic estimate would be obtained. So, the empirical "transition" values of $\Delta\xi/b = 0.01$, based on areas of influence, and $I_w/I_c = 1.01$, based on the pressure signature impulse, could be useful even though they had not been independently verified as the most general parametric indicators, or the indicators with the most reasonable values.

Inaccurate Lift Predictions And Scale Effects

The pressure plots in figure 20 indicated that agreement between predicted and measured surface pressures on the outer wing panel was rather poor. At the same time, the predicted and measured wing surface pressures, reference 22, showed reasonably good agreement on the inboard wing panels where the camber and twist was not severe and most of the lift was being developed. Comparisons of predicted and measured lift, drag, and pitching moment coefficients also showed close agreement over the range of angle of attack associated with supersonic-cruise flight.

Most of the low-boom tailored concepts and wind-tunnel models discussed had strakes or highly-swept leading edges on the inboard wing panels where most of the lift was generated, and where the Modified Linear Theory Method code predictions were reasonably accurate. Other comparisons made in references 22 and 29 showed that the Modified Linear Theory Method code predicted overall lift, drag, and pitching moment coefficients with reasonable accuracy over the range of angle of attack that included $C_{L,CRUISE}$. So, while the observation was true for some wing planforms (highly-swept, highly notched arrow wings), it might not be a serious problem for conceptual HSCT and/or SBJ wing planforms at their respective low cruise angles of attack.

This problem of poor agreement between predicted and measured surface pressures on the outboard wing panels of the highly-swept, highly notched arrow wings wind-tunnel models might be the result of too few "Mach boxes" (calculation panels) along the outer-panel chords of these particular wing planforms. The computer code presented and discussed in reference 22 originally allotted 2000 equally sized "Mach boxes" for the calculation of upper and lower surface pressures over half of the planform. Along the chords of the inner wing panels, there were dozens of "Mach boxes" available to define surface pressures along each chord. However, on the outboard wing panels where the chords were considerably shorter in length, there could be only ten or less "Mach boxes" that fit between the leading and trailing edges. Since the surface pressures were calculated and "smoothed", by numerical flow potential averaging, fewer chord stations resulted in locally poorer accuracy. The obvious solution was to significantly increase the number of "Mach boxes" spread over the wing planform for the calculation of surface pressures. This would improve the definition of force coefficients slightly on the inner wing panels where there were an abundance of "Mach boxes", but it would certainly increase the accuracy of the area-ruled surface

pressures on the outer wing panels where they significantly contributed to the lift equivalent area curve, near and at, its maximum point. Even with this update in place, caution in the use of the Modified Linear Theory Method for sonic-boom analysis was certainly advised.

While the aforementioned remedies might alleviate the problem of aerodynamic performance computational inaccuracies, they would do little to reduce the problem associated with wing tip stall on small wind-tunnel model wings with low taper ratios. Increasing the twist on the outer panels could get rid of tip stall on the wind-tunnel model, but it might be obtained by a reduction in the cruise lift / drag ratio of the full-scale concept. This design problem would need to be addressed on a case-by-case basis, since general suggestions based on limited data could aggravate rather than ameliorate the problem.

All of these effects, but especially the near-field effects, added extra difficulties to the task of measuring report-quality pressure signatures of low-boom-tailored models in the wind tunnel. Evaluating the merits of a low-boom concept design based on wind-tunnel model performance was now complicated by the need to thoroughly understand the physics of the three-dimensional flow-field disturbances produced by the model. This was especially true when near-field measured, or calculated, pressure signatures were to be used as input data for the Thomas Extrapolation Code, reference 26, to obtain predictions of ground signatures and overpressures.

Two options seemed possible: (1) build models small enough so that the separation distances at which pressure signatures were measured could be reasonably close to that limiting distance where far-field theory extrapolation methods could be applied; or (2) measure pressure signatures with large accurately-detailed models in wind tunnels with very large test sections for the same purposes of extrapolation. The use of small models, option (1), risked encountering and aggravating tip-stall effects if the wings were highly tapered. Measuring pressure signatures in wind tunnels with large test sections, option (2), would be very expensive. Whichever option was chosen, wind tunnel measurements of pressure signatures would have to be made, evaluated, and studied. If they indicated that low-boom-shaped pressure signatures would form and could be expected to persist to the ground, then the very expensive design and construction of a full-scale prototype could be proposed and submitted for funding.

Concluding Remarks

A qualitative empirical analysis of near-field flow physics and acoustics has indicated that lift-induced shocks could appear in the near-field pressure signatures of a lifting wing-fuselage concept or a wind-tunnel model at cruise attitude conditions. Two mathematical models, one obtained from the application of equations derived with geometric acoustics and the second with cross-flow theory to obtain lift/volume impulse ratios, were employed to study near-field flow properties. From the application of these models, it was concluded these shocks on the positive-pressure sections of the pressure signatures from properly-designed low-boom models would gradually attenuate and blend into the desired shapes of low-boom concept and model pressure signatures at a distance described by some "transition" distance-to span ratio. "Transition" distance-to-span ratios were predicted for four wind-tunnel models of supersonic-cruise concepts. The two empirically-derived distance ratio methods predicted transition distance ratios that varied from a $h/b = 6$ (which seemed low) for a Mach 3 concept to a $h/b = 23$ (which seemed somewhat large) for a Mach 1.8 concept. These transition distance ratios were found to be larger for concepts with arrow wings than for concepts with delta wings, and h/b (transition) values

determined from impulse ratio calculations were usually larger than those calculated with the geometric acoustic method. It was also possible that the ratio of lift equivalent areas to volume equivalent areas affected the likelihood that lift-induced shocks would appear and alter the desired shape of the low-boom-tailored signature in the wind-tunnel environment, but this factor was not addressed in this paper due to the sparsity of data from the small sample of HSCT and SBJ wind-tunnel models and their representative pressure signature data.

Two methods could be used to determine which of these two "transition distance" prediction techniques was more useful. The first method would used CFD codes to perform studies of pressure signature shape change at increasing separation distances to obtain a value of "transition" h / b. A second method would employ low-boom-tailored wind-tunnel model(s) which would be used to measure pressure signatures over a range of separation distances. Either, or both in tandem execution, could provide useful and definitive results.

The Modified Linear Theory wing performance analysis code could provide reasonably good predictions of aerodynamic force and pitching moment coefficients for conceptual aircraft wing planforms with small, but not excessively low, taper ratios. Calculations made with the largest number of available computational "Mach boxes" maximized the possibility that surface pressures on the inboard and outboard wing panels would be predicted with a accuracy sufficient for credible performance coefficient values and good sonic-boom equivalent area due to lift distributions. Possible tip stall tendencies on the low-boom wind-tunnel models would have to be considered during the wing planform design phase of the full-scale conceptual aircraft, and countered with careful applications of camber and twist along the semi-span.

The analysis, discussion, and conclusions of this study also indicated why extrapolating near-field - half to one span length separation distance - pressure signatures to the ground with codes based on the Thomas Code would not provide good ground overpressure predictions. There would be a serious physical mismatch between the two-dimensional, cylindrical propagation model, flow field of the Thomas Code, and the real three-dimensional flow-field around the concept or wind-tunnel model generating the pressure signature. The prediction of ground overpressures generated by lifting wing-fuselage models or concepts with this extrapolation method would be suspect because a distorted low-boom or an N-wave ground-level pressure signature shape could very likely be predicted whether the configuration was designed with low-boom methods or with mission-constrained methods. Such a result would discourage efforts to tailor the configuration's geometry with applications of Seebass and George Minimization Theory.

When pressure signatures measured at "transition distances" were extrapolated, however, the real and propagation model flow fields would be in much better accord, and credible predictions could be expected. Determination of "transition distances" at all Mach numbers and all types of supersonic-cruise vehicles would encourage the building of low-boom models with "realistic" features so that pressure signatures from them could be measured in wind tunnel test sections capable of providing the appropriate "transition distance" volumes.

References

1. Carlson, Harry W.: *An Investigation Of Some Aspects Of The Sonic Boom By Means Of Wind-Tunnel Measurements Of Pressures About Bodies At A Mach Number Of 2.01.* NASA TN D-161, December 1959.

2. Carlson, Harry W.: *An Investigation Of The Influence Of Lift On Sonic-Boom Intensity By Means Of Wind-Tunnel Measurements Of The Pressure Fields Of Several Wing-Body Combinations At A Mach Number Of 2.01.* NASA TN D-881, July 1961.

3. Morris, Odell A.: *A Wind-Tunnel Investigation At A Mach Number Of 2.01 Of The Sonic-Boom Characteristics Of Three Wing-Body Combinations Differing In Wing Longitudinal Location.* NASA TN D-1384, September 1962.

4. Carlson, Harry W.; and Shrout, Barrett L.: *Wind-Tunnel Investigation Of The Sonic-Boom Characteristics Of Three proposed Supersonic Transport Configurations.* NASA TM X-889, October 1963.

5. Carlson, Harry W.; Mack, Robert J.; and Morris, Odell A.: *A Wind-Tunnel Investigation Of The Effect Of Body Shape On Sonic-Boom Pressure Distributions.* NASA TN D-3106, November 1965.

6. Shrout, Barrett L.; Mack, Robert J.; and Dollyhigh, Samuel M.: *A Wind-Tunnel Investigation Of Sonic-Boom Pressure Distributions Of Bodies Of Revolution At Mach 2.96, 3.83, And 4.63*, NASA TN D-6195, April 1971.

7. Harris, Roy V., Jr.: *An Analysis And Correlation Of Aircraft Wave Drag.* NASA TM X-947, 1964.

8. Middleton, Wilbur D.; and Carlson, Harry W.: *A Numerical Method For Calculating Near-Field Sonic-Boom Pressure Signatures.* NASA TN D-3082, 1965.

9. Harris, Roy V., Jr.: *A Numerical Technique For Analysis Of Wave Drag At Lifting Conditions.* NASA TN D-3586, 1966.

10. Craidon, Charlotte B.: *Description Of A Digital Computer Program For Airplane Configuration Plots.* NASA TM X-2074, 1970.

11. Whitham, G. B.: *The Flow Pattern of a Supersonic Projectile.* Communications on Pure and Applied Mathematics vol. V, no. 3, August 1952, pp. 301-348.

12. Walkden, F.: *The Shock Pattern of a Wing-Body Combination, Far From the Flight Path.* Aeronautical Quarterly, vol. IX, pt. 2, May 1958, pp. 164-194.

13. Mack, Robert J.; and Darden, Christine M.: *Wind-Tunnel Investigation Of The Validity Of A Sonic-Boom Minimization Concept.* NASA TP-1421, 1979.

14. Mack, Robert J.; and Needleman, Kathy E.: *The Design Of Two Sonic Boom Wind Tunnel Models From Conceptual Aircraft Which Cruise At Mach Numbers Of 2.0 And 3.0.* AIAA-90-4026, AIAA 13th Aeroacoustics Conference, October 22-24, 1990.

15. Mack, Robert J.: *An Analysis Of Measured Pressure Signatures From Two Theory-Validation Low-Boom Models.* NASA / TM-2003-212423, October 2003

16. Haglund, George T.: *Low Sonic Boom Studies At Boeing*. High-Speed Research: Sonic Boom, Volume II, NASA Conference Publication 10133, 1993.

17. Baize, Daniel G.; and Coen, Peter G.: *A Mach 2.0 / 1.6 Low Sonic Boom High-Speed Civil Transport Concept.* High-Speed Research: Sonic Boom, Volume II, NASA Conference Publication 10133, 1993.

18. Mack, Robert J.: *Low-Boom Aircraft Concept With Aft-Fuselage-Mounted Engine Nacelles.* High-Speed Research: Sonic Boom, Volume II, NASA Conference Publication 10133, 1993.

19. Mack, Robert J.: *Wind-Tunnel Overpressure Signatures From A Low-Boom HSCT Concept With Aft-Fuselage-Mounted Engines*. High-Speed Research: 1994 Sonic Boom Workshop, Configuration Design, Analysis, and Testing. NASA / CP-1999-209699, December 1999.

20. Mack, Robert J.: *A Supersonic-Cruise Business Jet Concept Designed For Low Sonic Boom.* NASA / TM-2003-212435, October 2003

21. Mack, Robert J.: *An Analysis Of Measured Sonic-Boom Pressure Signatures From A Langley Wind Tunnel Model Of A Supersonic-Cruise Business Jet Concept.* NASA / TM-2003-212447, October 2003.

22. Carlson, Harry W.; and Mack, Robert J.: *Estimation Of Wing Nonlinear Aerodynamic Characteristics at Supersonic Speeds*. NASA TP-1718, 1980.

23. Mack, Robert J.: *Some Considerations On The Integration Of Engine Nacelles Into Low-Boom Aircraft Concepts*. High-Speed Research: Sonic Boom, Volume II, NASA Conference Publication 3173, February 1992.

24. Mack, Robert J.; and Darden, Christine M.: *Limitations On Wind-Tunnel Pressure Signature Extrapolation*. High-Speed Research: Sonic Boom, Volume II, NASA Conference Publication 3173, February 1992.

25. Seebass, R.; and George, A. R.: *Sonic-Boom Minimization.* Journal of the Acoustical Society of America, vol. 51, no. 2, pt. 3, February 1972, pp. 686 - 694.

26. Thomas, Charles L.: *Extrapolation Of Wind-Tunnel Sonic Boom Signatures Without Use Of A Whitham F-function*. Third Conference on Sonic Boom Research, NASA SP-255, 1971.

27. Middleton, Wilbur D.; and Carlson, Harry W.: *Numerical Method For Estimating And Optimizing Supersonic Aerodynamic Characteristics Of Arbitrary Planform Wings.* Journal of Aircraft, vol. 2, no. 4, July-August 1965, pp. 261-265.

28. Mack, Robert J.; and Haglund, George T.: *A Practical Low-Boom Overpressure Signature Based On Minimum Sonic Boom Theory.* High-Speed Research: Sonic Boom, Volume II, NASA Conference Publication 3173, February 1992.

29. Carlson, Harry W.; and Mann, Michael J.; *Survey And Analysis Of Research On Supersonic Drag-Due-To-Lift Minimization With Recommendations For Wing Design.* NASA TP-3202, September 1992.

30. Carlson, Harry W.: *Pressure Distributions At Mach Number 2.05 On A Series Of Highly Swept Arrow Wings Employing Various Degrees Of Camber And Twist.* NASA TN D-1264, 1962.

Appendix A

Description Of The Mach 2 And The Re-sized Mach 3 Low-Boom Concepts

The Mach 2 and Mach 3 concepts were designed to validate the low-sonic-boom analysis and design methods that had been developed prior to the close of the SCAT and SCAR programs. Volume and lift distributions of both conceptual aircraft were tailored to generate low-boom shaped pressure signatures and ground-level overpressures of about 1.0 psf while cruising at their respective design Mach numbers, cruise altitudes, and beginning-cruise weights. No attempts were made to size the concepts' wing planforms for enhanced mission performance or for minimum structural weights. However, the wing area on the initial Mach 3 concept was downsized from 16,605.0 ft^2 to 13, 450.1 ft^2 to keep it at or below that of the Mach 2 concept .

	Mach 2 Concept	Mach 3 Concept
Span, ft	160.0	129.6
Length, ft	313.0	330.0
Wing Lift Length, ft	300.0	300.0
Wing Area, ft^2	15,055.0	13,450.1
Aspect Ratio, b^2/S	1.70	1.25
Cruise Altitude, ft	55,000.0	65,000.0
Beginning Cruise Weight, lb	550,000.0	550,000.0
Beginning Cruise Weight / Wing Area	36.5	40.9
$C_{L,CRUISE}$	0.06803	0.05457
Cruise Mach Number	2.0	3.0
Number Of Engines	4	4
Ground-Level Overpressure, psf	1.0	1.0
Low-Boom Pressure Signature Shape, reference 25	"Flat-top"[1]	"Ramp"[1]

1. See reference 25 for a description of "Flat-top" and "Ramp" overpressure signature shapes

Appendix B

Data From The Three Follow-On Low-Boom Concepts.

These concepts were designed during the High Speed Research (HSR) program. They were required to meet low-boom constraints, mission-range performance, takeoff and landing field length limits (balanced field length was not set), and center-of-gravity limits.

	B935[1]	LB-16[2]	HSCT-10B[3]
Low-Boom Mach Number	1.7	1.6	1.8
Ground Δp at Start of Cruise, psf	1.0	1.0	1.0
Over-Water Mach Number	2.4	2.0	2.4
Mission Range, nmi	5,000	6,500	5,000
Wing Area, ft^2	9,000	9,263	10,465
Wing Span, ft	140	140	150
Aspect Ratio, $Span^2$ / Area	2.18	2.12	2.15
Length, ft	317	295	328
Gross Takeoff Weight, lb	731,600	646,356	662,000
Beginning Cruise Weight, lb	650,000	609,000	618,000
Beginning Cruise Altitude, ft	44,000	47,650	49,300
$C_{L,CRUISE}$ at Low-Boom Mach Number	0.11742	0.13458	0.10335
A_E, Lift at Start of Cruise, ft^2	680.4	778.5	800.5
Beginning Cruise Weight / Wing Area, psf	72.2	65.7	59.1
Empty Weight, lb	319,300	203,310	246,000
Number of Passengers	300	250	300
Gross Takeoff Weight / Empty Weight	2.29	3.18	2.69
Shape of Pressure Signature	"Hybrid"[4]	"Ramp"	"Hybrid"[4]

1. Reference 16
2. Reference 17
3. Reference 18
4. See reference 25 for a description of the "ramp" pressure signature, and reference 28 for description of the "Hybrid" pressure signature.

Appendix C

Three-view Sketches Of The B935 and LB16

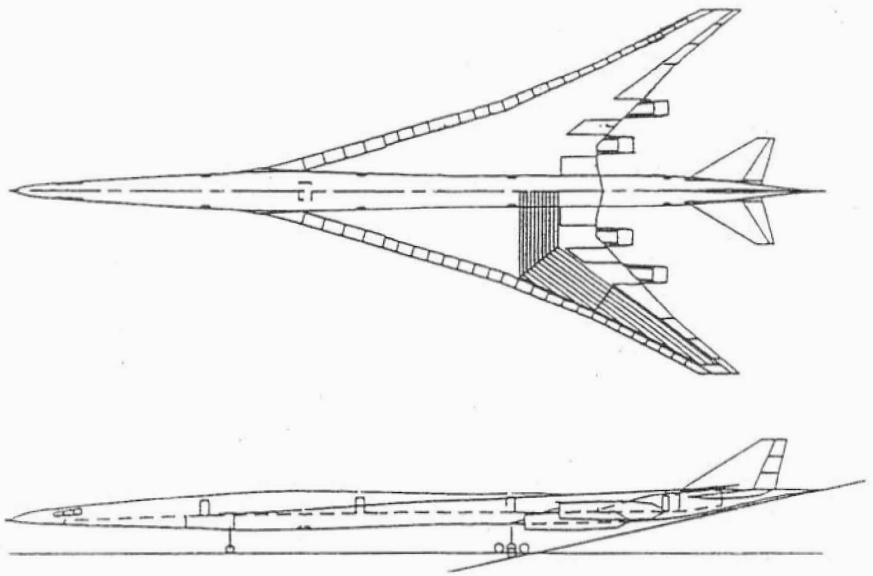

Figure C1. Two-view sketch of the B935 concept.

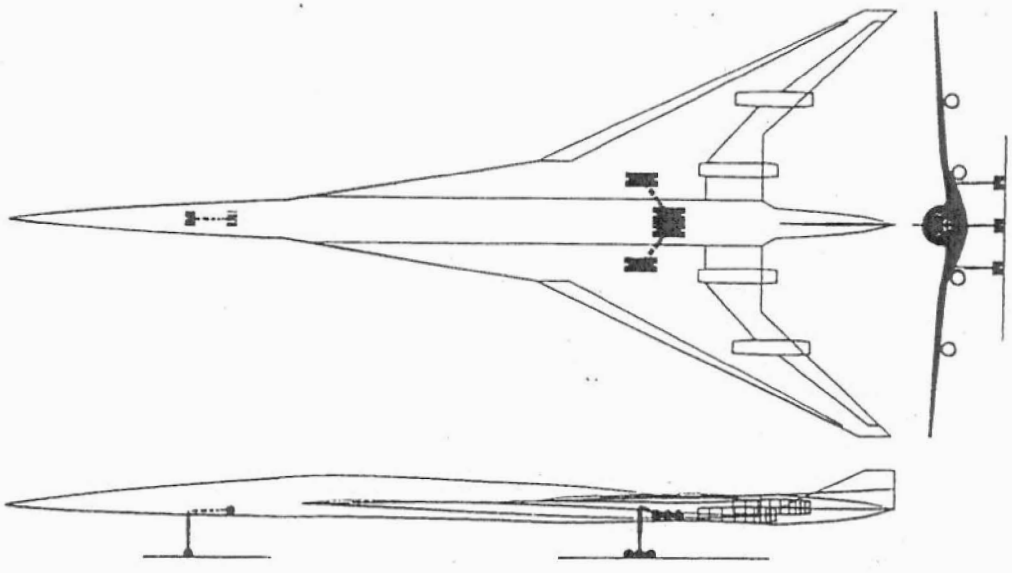

Figure C2. Three-view sketch of the LB16 concept.

Appendix D

HSCT-10B Engine Nacelles

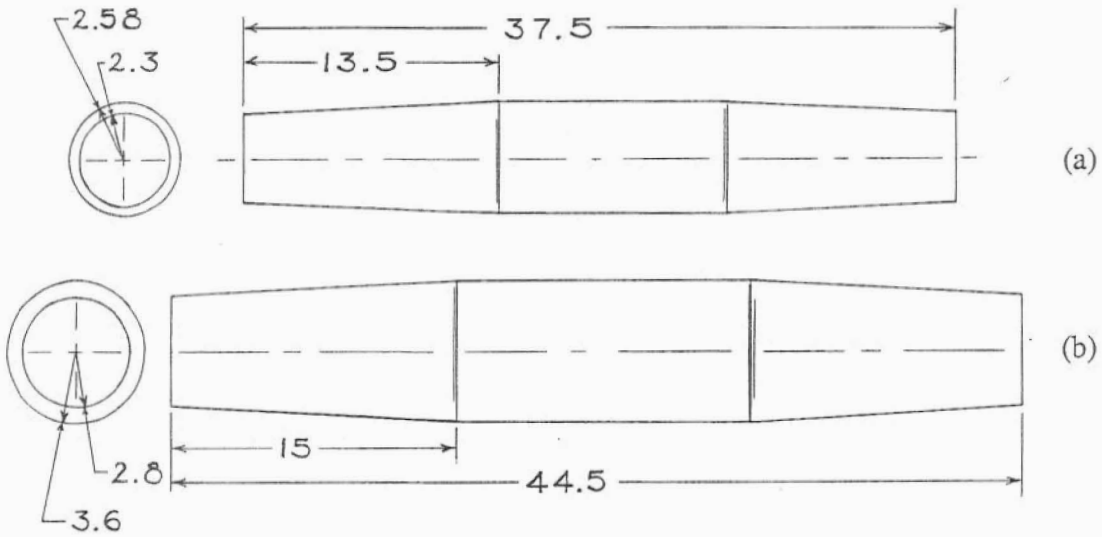

Nacelle (a) was sized to enclose an advanced technology, high performance turbojet engine that had little or no noise constraints.

Nacelle (b) was sized to enclose a more "realistic"engine, one more like the engines proposed for the supersonic-cruise conceptual aircraft designed during the HSCT and HSR Programs.

Appendix E

Langley Low-Boom Business Jet Concept

Design Data[1]

Span, ft.	55.0
Overall Length, ft.	132.5
Wing Area (reference), ft.^{2}	1,560.25
Wing Aspect Ratio (projected area)	1.93
Number of Engines	2
Number of Passengers	10
Shape of Pressure Signature	"Hybrid"[2]

Mission Data[1]

Cruise Mach Number	2.0
Range, nmi.	4,000.0
Ground Δp at Start Of Cruise, psf	0.5
Beginning Cruise Altitude, ft.	53,000.0
C_L at Cruise Mach Number	0.09597
Gross Takeoff Weight, lb.	99,435.0
Beginning Cruise Weight, lb.	88,497.0
Beginning Cruise Weight / Wing Area, psf	56.7
Mission Fuel Weight, lb.	55,302.0
Empty Weight, lb.	41,514.0
Gross Takeoff Weight / Empty Weight	2.4

1. Further design details are found in reference 20.
2. See reference 28 for a description and a discussion of the "Hybrid" pressure signature.

REPORT DOCUMENTATION PAGE

Form Approved
OMB No. 0704-0188

1. REPORT DATE *(DD-MM-YYYY)*	2. REPORT TYPE	3. DATES COVERED *(From - To)*
01- 08 - 2006	Technical Memorandum	

4. TITLE AND SUBTITLE

Anomalous Shocks on the Measured Near-Field Pressure Signatures of Low-Boom Wind-Tunnel Models

5a. CONTRACT NUMBER

5b. GRANT NUMBER

5c. PROGRAM ELEMENT NUMBER

6. AUTHOR(S)

Mack, Robert J.

5d. PROJECT NUMBER

5e. TASK NUMBER

5f. WORK UNIT NUMBER

984754.02.07.07

7. PERFORMING ORGANIZATION NAME(S) AND ADDRESS(ES)

NASA Langley Research Center
Hampton, VA 23681-2199

8. PERFORMING ORGANIZATION REPORT NUMBER

L-19196

9. SPONSORING/MONITORING AGENCY NAME(S) AND ADDRESS(ES)

National Aeronautics and Space Administration
Washington, DC 20546-0001

10. SPONSOR/MONITOR'S ACRONYM(S)

NASA

11. SPONSOR/MONITOR'S REPORT NUMBER(S)

NASA/TM-2006-214496

12. DISTRIBUTION/AVAILABILITY STATEMENT

Unclassified - Unlimited
Subject Category 71
Availability: NASA CASI (301) 621-0390

13. SUPPLEMENTARY NOTES

An electronic version can be found at http://ntrs.nasa.gov

14. ABSTRACT

Unexpected shocks on wind-tunnel-measured pressure signatures prompted questions about design methods, pressure signature measurement techniques, and the quality of measurements in the flow fields near lifting models. Some of these unexpected shocks were the result of component integration methods. Others were attributed to the three-dimension nature of the flow around a lifting model, to inaccuracies in the prediction of the area-ruled lift, or to wing-tip stall effects. This report discusses the low-boom model wind-tunnel data where these unexpected shocks were initially observed, the physics of the lifting wing/body model's flow field, the wind-tunnel data used to evaluate the applicability of methods for calculating equivalent areas due to lift, the performance of lift prediction codes, and tip stall effects so that the cause of these shocks could be determined.

15. SUBJECT TERMS

Supersonic flow; Sonic boom; Wind-tunnel tests; Near-field shocks

16. SECURITY CLASSIFICATION OF:			17. LIMITATION OF ABSTRACT	18. NUMBER OF PAGES	19a. NAME OF RESPONSIBLE PERSON
a. REPORT	b. ABSTRACT	c. THIS PAGE			STI Help Desk (email: help@sti.nasa.gov)
					19b. TELEPHONE NUMBER *(Include area code)*
U	U	U	UU	42	(301) 621-0390